1521-0111/12/8203-448–463$25.00
MOLECULAR PHARMACOLOGY
Vol. 82, No. 3
79137/3787933

Mol Pharmacol 82:448–463, 2012

Computational and Experimental Analysis of the Transmembrane Domain 4/5 Dimerization Interface of the Serotonin 5-HT_{1A} Receptor[S]

Nataliya Gorinski, Noga Kowalsman, Ute Renner, Alexander Wirth, Michael T. Reinartz, Roland Seifert, Andre Zeug, Evgeni Ponimaskin, and Masha Y. Niv

Cellular Neurophysiology, Medical School Hannover, Germany (N.G., A.W., A.Z., E.P.); Institute of Biochemistry, Food Science and Nutrition, the Robert H. Smith Faculty of Agriculture, Food and Environment, and the Fritz Haber Center for Molecular Dynamics, the Hebrew University of Jerusalem, Israel (N.K., M.Y.N.); DFG-Research Center for the Molecular Physiology of the Brain (CMPB), Göttingen, Germany (U.R., E.P.); and Institute of Pharmacology, Medical School Hannover, Germany (M.T.R., R.S.)

Received April 4, 2012; accepted June 5, 2012

ABSTRACT

Experimental evidence suggests that most members of class A G-protein coupled receptors (GPCRs) can form homomers and heteromers in addition to functioning as single monomers. In particular, serotonin (5-HT) receptors were shown to homodimerize and heterodimerize with other GPCRs, although the details and the physiological role of the oligomerization has not yet been fully elucidated. Here we used computational modeling of the 5-HT_{1A} receptor monomer and dimer to predict residues important for dimerization. Based on these results, we carried out rationally designed site-directed mutagenesis. The ability of the mutants to dimerize was evaluated using different FRET-based approaches. The reduced levels of acceptor photobleaching-Förster resonance energy transfer (FRET) and the lower number of monomers participating in oligomers, as assessed by lux-FRET, confirmed the decreased ability of the mutants to dimerize and the involvement of the predicted contacts (Trp175$^{4.64}$, Tyr198$^{5.41}$, Arg151$^{4.40}$, and Arg152$^{4.41}$) at the interface. This information was reintroduced as constraints for computational protein-protein docking to obtain a high-quality dimer model. Analysis of the refined model as well as molecular dynamics simulations of wild-type (WT) and mutant dimers revealed compensating interactions in dimers composed of WT and W175A mutant. This provides an explanation for the requirement of mutations of Trp175$^{4.64}$ in both homomers for disrupting dimerization. Our iterative computational-experimental study demonstrates that transmembrane domains TM4/TM5 can form an interaction interface in 5-HT_{1A} receptor dimers and indicates that specific amino acid interactions maintain this interface. The mutants and the optimized model of the dimer structure may be used in functional studies of serotonin dimers.

Introduction

The 5-hydroxytryptamine (5-HT, serotonin) system in the brain is involved in multiple processes, including regulation of neurogenesis, neuronal activity, as well as respiratory and cardiovascular control (Richter et al., 2003) and energy balance (Lam and Heisler, 2007).

Serotonin receptors, with the exception of the 5-HT_3 ion channel, are G-protein-coupled receptors (GPCRs), a large and diverse family of membrane proteins that participate in regulating cellular and physiological processes and represent key pharmacological targets. The 5-HT_{1A} receptor subtype is involved in processes such as the regulation of neurogenesis, temperature control, and regulation of sleep. Particular interest in this receptor has been raised as a result of its involvement in regulating depression and anxiety states (Lesch and Gutknecht, 2004).

This work was funded by the Niedersachsen-Israel research fund [Grant ZN2448] and Deutsche Forschungsgemeinschaft [Grant PO732].
N.G. and N.K. contributed equally to this work.
Article, publication date, and citation information can be found at http://molpharm.aspetjournals.org.
http://dx.doi.org/10.1124/mol.112.079137.
[S] The online version of this article (available at http://molpharm.aspetjournals.org) contains supplemental material.

ABBREVIATIONS: 5-HT, 5-hydroxytryptamine (serotonin); GPCR, G-protein-coupled receptor; FRET, Förster resonance energy transfer; TM, transmembrane; 3D, three-dimensional; PDB, Protein Data Bank; MD, molecular dynamics; GFP, green fluorescence protein; 8-OH-DPAT, 8-hydroxy-2-dipropylaminotetralin; PAGE, polyacrylamide gel electrophoresis; YFP, yellow fluorescent protein; WT, wild type; CFP, cyan fluorescent protein; IL, intracellular loop; vdW, van der Waals; RMSD, root-mean-square deviation; D3, dopamine D_3 receptor; OR, opioid receptor; PNGase, glycopeptidase; ER, endoplasmic reticulum; lux-FRET, linear unmixing FRET.

In the last decade, it has become clear that many GPCRs may function as dimers or higher order oligomers (Woehler et al., 2009; Albizu et al., 2010; Lohse, 2010; Ganguly et al., 2011; Rozenfeld and Devi, 2011). Oligomerization has implications for trafficking, signaling, and pharmacology of many members of the GPCR family, but in many cases, the functional implications of GPCR oligomerization still need to be delineated.

We have demonstrated that 5-HT$_{1A}$ receptors form homodimers at the plasma membrane (Kobe et al., 2008; Woehler et al., 2009). The analysis of 5-HT$_{1A}$ receptor oligomerization dynamics by combined FRET approaches revealed that receptor stimulation results in accumulation of FRET-negative complexes rather than in dissociation of oligomers to monomers. The oligomerization of 5-HT$_{1A}$ receptors was shown to be constitutive (Ganguly et al., 2011), the oligomerization status being independent of ligand stimulation but enhanced as a result of acute (but not chronic) cholesterol depletion (Paila et al., 2011a). Despite these advances and computational work on monomers (Paila et al., 2011b), the interaction interface of 5-HT$_{1A}$ dimers remains unknown and is the focus of the current article.

Almost every transmembrane (TM) domain within the GPCR has been suggested to mediate the dimeric interactions, but TM domains 4 and/or 5 have gained the most support as dimerization interfaces (González-Maeso et al., 2008; Johnston et al., 2011; Hu et al., 2012). The TM4/TM5 interface is also compatible with images obtained via atomic force microscopy [Fotiadis et al., 2003; Protein Data Bank (PDB) ID 1N3M]. Specifically, the extracellular part of TM4 was found to be involved in oligomerization by site-directed cysteine cross-linking studies in dopamine D$_2$ receptor homodimers (Guo et al., 2003), in 5-HT$_{2C}$ (Mancia et al., 2008), and in the yeast STE2 receptor (Wang and Konopka, 2009).

In the present study, we aimed to establish a working model of the three-dimensional structure of the complex. As a first step, we constructed 3D models of 5-HT$_{1A}$ receptor monomer, as described for modeling of other GPCRs (Yarnitzky et al., 2010; Levit et al., 2012).

The monomer models were fitted into the TM4/TM5 dimeric model of rhodopsin (PDB ID 1N3M). On the basis of analysis of the residues contributing to the dimeric interaction in these models, we designed dimerization-disrupting mutations. We then carried out site-directed mutagenesis and monitored the dimerization levels of the mutants using different FRET-based approaches. The confirmed interactions were introduced as constraints in protein-protein docking of monomers, and the optimized dimeric models were analyzed. The best model of WT dimer and the models of the mutant receptor dimers were submitted to molecular dynamics (MD) simulations. These simulations rationalize the mutagenesis results and provide a detailed view of the interaction interface. The results of our study 1) confirmed the existence of the TM4/TM5 dimer interface for 5-HT1A, 2) enabled us to refine the model of the dimer, and 3) provided pharmacologically intact, dimerization-impaired 5-HT$_{1A}$ monomers, an important tool for further functional studies of 5-HT$_{1A}$ receptor dimerization. After the completion of our work, a structure by Manglik et al. (2012) revealed that the μ-opioid receptor (μ) crystallizes as a 2-fold symmetrical dimer through a four-helix bundle motif formed by transmembrane segments 5 and 6. The serotonin dimer proposed in the current work, is theoretically capable of coexistence with the opioid-like 5,6 dimer.

Materials and Methods

Recombinant DNA Procedures

The construction of 5-HT$_{1A}$ receptors fused to different spectral variants of the green fluorescence protein (GFP) has been described previously (Renner et al., 2007). The mutagenesis of potential interaction sites within 5-HT$_{1A}$ receptor was performed using a site-directed mutagenesis kit (Stratagene, La Jolla, CA) according to the manufacturer's protocol. The following primers were used: W136A/D140A: sense, 5′-GCG CTA GAC AGG TAC GCG GCA ATC ACC GCC CCT ATA GAC TAC GTG-3′; antisense, 5′-CAC GTA GTC TAT AGG GGC GGT GAT TGC CGC GTA CCT GTC TAG CGC-3′; L159A/L166A: sense, 5′-GCG CTG ATC TCG GCC ACT TGG CTC ATT GGC TTT GCC ATC TCC ATC CC-3′; antisense 5′-GGG ATG GAG ATG GCA AAG CCA ATG AGC CAA GTG GCC GAG ATC AGC GC-3′; W175A: sense, 5′-CGC CTA TGC TGG GCG CGC GCA CCC CGG AAG-3′; antisense, 5′-CTT CCG GGG TGC GCG CGC CCA GCA TAG GCG-3′; R151K/R152K: sense 5′-CAA GAG GAC GCC CAA GAA GGC CGC TGC GCT GAT C-3′; antisense, 5′-GAT CAG CGC AGC GGC CTT CTT GGG CGT CCT CTT G-3′; R176K: sense, 5′-GCC TAT GCT GGG CTG GAA GAC CCC GGA AGA CCG C-3′; antisense, 5′-GCG GTC TTC CGG GGT CTT CCA GCC CAG CAT AGG C-3′; Y198F: sense, 5′-CGG GTA CAC CAT CTT CTC CAC TTT CGG CGC-3′; antisense, 5′-GCG CCG AAA GTG GAG AAG ATG GTG TAC CCG-3′. All mutants were verified by double-stranded dideoxy DNA sequencing at the level of the final plasmid.

Adherent Cell Culture and Transfection

Mouse N1E-115 neuroblastoma cells from the American Type Culture Collection (Manassas, VA) were grown in Dulbecco's modified Eagle's medium containing 10% fetal calf serum and 1% penicillin/streptomycin at 37°C under 5% CO_2. For transient transfection, cells were seeded at low density in 60-mm dishes (10^6) or on 10-mm cover-slips (5×10^5) and transfected with appropriate vectors using Lipofectamine 2000 Reagent (Invitrogen, Carlsbad, CA) according to the manufacturer's instruction. Four hours after transfection, cells were serum-starved overnight before analysis. The amount of expressed receptor was measured in membrane preparations of transfected cells by using radioactive ligand binding assay with [^{3}H]8-OH-DPAT as a specific ligand and nonradioactive 5-HT as a competitor.

Expression and Glycosylation of 5-HT$_{1A}$ Receptor WT and Interaction Interface Mutants

Twenty-four hours after transfection, cells were washed in phosphate-buffered saline, lysed with 100 μl of Laemmli loading buffer, and 15 μl of each sample were separated by 10% SDS-PAGE under reducing conditions. To analyze the glycosylation profile, lysates were prepared and treated with endoglycosidase (Endo) H and glycopeptidase (PNGase) F according to the manufacturer's protocol (New England Biolabs, Ipswich, MA). In brief, cells transfected with yellow fluorescent protein (YFP)-tagged 5-HT$_{1A}$ receptor were lysed in glycoprotein denaturing buffer and then treated with 1.000 U of corresponding glycosidase (EndoH or PNGase-F) along with untreated controls for 1 h at 37°C. Finally, samples were separated by 10% SDS-PAGE under reducing conditions. YFP- or GFP-tagged constructs were visualized after SDS-PAGE directly in the gel by using variable mode imager Typhoon 9400 (GE Healthcare, Chalfont St. Giles, Buckinghamshire, UK). For that, gels were excited at λ_{ex} 488 nm, and emission was collected by using a band-pass filter 530 BP 25.

Radioligand Binding Assay

Membrane preparation of transiently transfected N1E cells was performed as described previously (Renner et al., 2007) and stored at −80°C until used. For the competition binding assay, membranes were thawed and resuspended in binding buffer (75 mM Tris/HCl, 12.5 mM $MgCl_2$, and 1 mM EDTA, pH 7.4) resulting in a final protein concentration of 0.72 μg/μl. Membranes were homogenized by using a 22-gauge needle (10 times) followed by a 27-gauge needle (15 times). Test tubes with a total reaction volume of 500 μl contained membranes with 18 μg of protein, 8-OH-DPAT (Tocris, Minneapolis, MN) at increasing concentrations, and [^{3}H]8-OH-DPAT (Hartmann Analytics, Braunschweig, Germany) at a final concentration of 1 nM. Reactions were shaken at 250 rpm at room temperature for 90 min to establish equilibrium. Separation of bound and free [^{3}H]8-OH-DPAT was achieved by filtration through glass-fiber filters [grade GF/C, presoaked with 0.3% (v/v) polyethylenimine in binding buffer; Whatman, Maidstone, UK] followed by three washing steps each with 2 ml of ice-cold binding buffer using a 48-well harvester (Brandel, Inc., Gaithersburg, MD) Radioactivity was measured by liquid scintillation counting using Rotiszint eco plus cocktail (Carl Roth GmbH, Karlsruhe, Germany). Data were analyzed by nonlinear regression functionality of Prism 5.0 (GraphPad Software, San Diego, CA).

Confocal Imaging and Single-Cell Acceptor Photobleaching FRET Analysis

Images of N1E-115 cells expressing WT and different mutants of 5-HT$_{1A}$-CFP and 5-HT$_{1A}$-YFP fusion proteins were acquired with an LSM780-Meta confocal microscope (Carl Zeiss, Jena, Germany) equipped with a 40×/1.3 numerical aperture oil-immersion objective at 512 × 512 pixels. The 458 nm line of a 40-mW argon laser was used at 15% power. Fluorescence emission was acquired from individual cells over 14 λ channels, in 10.7-nm steps, ranging from 475 to 625 nm. For each measurement, a series of eight images was acquired over a duration of 124 s. After the fourth image acquisition, bleaching of the acceptor (YFP) was performed in a selected 20 × 20-pixel region of interest in the plasma membrane. For that, the 514 nm line of the Argon laser was used, set at 50% power and 100% transmission for 300 scanning interactions using a 458 nm/514 nm dual dichroic mirror. Linear unmixing was performed by the Zeiss AIM software package using CFP and YFP reference spectra. Reference spectra were obtained from images of cells expressing only 5-HT$_{1A}$-CFP or 5-HT$_{1A}$-YFP acquired with the acquisition settings mentioned above. Apparent FRET efficiency was calculated offline using the equation

$$Ef_D = 1 - \left(\frac{F_{DA}}{F_D}\right) \quad (1)$$

where f_D is the fraction of donor participating in the FRET complex (i.e., ratio of FRET complexes over a total donor concentration, [DA]/[D^t]), F_{DA} and F_D are the background-subtracted and acquisition bleaching-corrected pre- and postbleach CFP fluorescence intensities, respectively. The acquisition bleaching-corrected postbleach CFP intensities were calculated as

$$F_D = F_D^{B,post} + \left(\frac{F_D^{R,pre} - F_D^{R,pre}}{F_D^{R,pre}}\right) F_D^{B,pre} \quad (2)$$

where F_D^B and F_D^R refer to CFP intensities of the bleach and reference region of interest, respectively, and "pre" and "post" refer to pre- and postbleach measurements.

Spectral Lux-FRET Analysis in Living Cells

Mouse N1E-115 neuroblastoma cells were cotransfected with plasmid DNAs encoding for WT and/or mutated 5-HT$_{1A}$ receptors fused with CFP and YFP. Sixteen hours after transfection, cells were resuspended in phosphate-buffered saline. All measurements were performed in 5-mm pathway quartz cuvettes using a spectrofluorometer (Fluorolog; Horiba Jobin Yvon, Edison, NJ) equipped with xenon lamp (450 W, 950 V). The cell suspension was stirred with a magnetic stirrer and the temperature was maintained at 37°C during the experiment. For calibration measurements, cells were cotransfected with plasmid encoding a single fluorophore-tagged 5-HT$_{1A}$ receptor together with an equal amount of plasmid encoding HA-tagged 5-HT$_{1A}$ receptor. During the time-course experiments, two emission spectra were obtained for each time point by exciting at 458 and 488 nm with 5 nm of spectral resolution for excitation and emission, respectively, and 0.5 s integration time. The spectral contributions from light scattering and nonspecific fluorescence of the cells were taken into account by subtracting the emission spectra of nontransfected cells (background) from each measured spectra. Before each measurement, the spectrofluorometer was calibrated for the xenon-lamp spectrum and Raman scattering peak position.

To determine apparent FRET efficiency for WT and mutants of the 5-HT$_{1A}$ receptor, we used a method described in detail by Wlodarczyk et al. (2008). This allows for a calculation of the total concentration ratio [A^t]/[D^t] of donor and acceptor, a donor molar fraction x_D = [D^t]/([D^t]+[A^t]) as well as the apparent FRET efficiencies Ef_D and Ef_A, where f_D = [DA]/[D^t] and f_A = [DA]/[A^t] are the fractions of donors and acceptors in complexes, respectively.

A model characterizing apparent FRET efficiency, Ef_D, as a function of donor mole fraction, x_D, for oligomeric structures has been developed previously (Veatch and Stryer, 1977):

$$Ef_D = E(1 - x_d^{n-1}) \quad (3)$$

Fitting this model to experimental data allows for the estimation of the true transfer efficiency, E, and also provides information about the number of units, n, interacting in the oligomeric complex. This model has been slightly augmented for use with Ef_A (Meyer et al., 2006):

$$Ef_A = E\frac{x_d}{1 - x_d}(1 - x_d^{n-1}) \quad (4)$$

Modeling the 5-HT$_{1A}$ Monomer

The mouse 5-HT$_{1A}$ receptor sequence (UniProtKB accession no. Q64264; see Supplemental Methods) was extracted from the UniProt server using the UniProtKB database. This sequence was used for modeling the 5-HT$_{1A}$ monomers by two protein structure prediction automated servers: M4T (http://manaslu.aecom.yu.edu/M4T/) (Fernandez-Fuentes et al., 2007) and I-TASSER (http://zhanglab.ccmb.med.umich.edu/I-TASSER/) (Roy et al., 2010). M4T builds 3D models of proteins by comparative modeling using a combination of multiple templates and iterative optimization of alternative alignments. The output of M4T produced a single model that was used in this study (termed TRP_out1, in which Trp175$^{4.64}$ pointed toward the outer surface of TM4). I-TASSER assembles 3D models based on multiple-threading alignments and iterative TASSER assembly simulations. I-TASSER returns up to five models. The model ranked 1 (best score) by I-TASSER was chosen as a monomer unit (termed TRP_in1, in which Trp175$^{4.64}$ pointed into the TM bundle); see Table 1. With the recent release of several new GPCR structures, we reused both M4T and I-TASSER for creating new monomers. The top-ranking model from I-TASSER (termed TRP_in2, "in" and "out" describing the Trp175 orientation), the third best model from I-TASSER (TRP_out3), and the M4T model (TRP_out2) were used in the subsequent analysis as well. The models are listed in Table 1, and the references for the GPCR templates used in their construction appear in the Supplemental Methods.

Intracellular loop 3 (IL3) in 5-HT$_{1A}$ receptor contains more than 100 residues (residues 218–345 as defined by the UniProtKB server). This is a unique feature of 5-HT$_{1A}$ receptor compared with the rest of the 5-HT receptors. The protein disorder prediction for IL3 was predicted using the PrDOS (Protein DisOrder prediction System) server (Ishida and Kinoshita, 2007; http://prdos.hgc.jp/cgi-bin/top.cgi). The se-

TABLE 1
The 5-HT$_{1A}$ models used in this study
The table show for each model the server that was used for preparing it. The "+" sign is used to designate early and subsequent models that were created after the appearance of additional GPCR X-ray structures in 2009. The references for the papers describing the template structures appear in Supplemental Methods.

	TRP_out1	TRP_out2	TRP_out3	TRP_in1	TRP_in2
Created by server	M4T	M4T	I-TASSER	I-TASSER	I-TASSER
Early [2009, 2010]	+			+	
Subsequent [end of 2010, 2011]		+	+		+
PDB IDs of templates used	2RH1	2RH1, 3D4S, 3EML	3PBL, 2RH1, 3NY8, 3EML	2RH1, 3D4S, 3EML	3PBL, 2RH1, 3NY8, 3EML

quence of mouse IL3 (residues 218–345) was given as input to the server using default values. The output shows predictions of ordered and disordered regions in IL3 at a 5% false positive rate. Moreover, in the templates used for modeling the 5-HT$_{1A}$ monomer (and other available GPCR structures), IL3 is either missing or replaced by the T4-lyzozyme domain; hence, no appropriate template structure can be found for this loop, and the modeled structure of IL3 in the 5-HT$_{1A}$ receptor models could not be considered reliable. Therefore, in our models, residues 233 to 330 were cut out, and the remaining ends of IL3 were connected. The resulting short loop was refined using the loop refinement protocol in Discovery-Studio 2.5 (Accelrys, Inc.) by using the default parameters.

Preliminary Modeling of 5-HT$_{1A}$ Receptor Homodimers

Homodimers of 5-HT$_{1A}$ receptor were obtained by superposing the monomer model on the structure of a putative Rhodopsin dimer (PDB ID 1N3M) (Fotiadis et al., 2003; Liang et al., 2003). The superposition was done for the TM helixes only and was based on sequence alignment of 5-HT$_{1A}$ receptor and rhodopin using Discovery Studio 2.5 (Accelrys, Inc.). Sequence alignment of mouse 5-HT$_{1A}$ receptor and rhodopsin was prepared using the alignment procedure of the UniProtKB server, which uses the ClustalW algorithm. The definitions of the TMs were taken from the UniProtKB server.

The homodimers were then analyzed for detecting important residues in the interface by the FastContact version 2.0 (http://structure.pitt.edu/servers/fastcontact/) (Camacho and Zhang, 2005) and COILCHECK (http://caps.ncbs.res.in/coilcheck/) (Alva et al., 2008) servers. The output of these servers lists the energy contribution of different residues in the interface to the interaction energy. For the refined dimers we also conducted an alanine scan using the Robetta server (http://robetta.bakerlab.org/alascansubmit.jsp) (Kortemme et al., 2004).

A detailed analysis of the interactions that a specific residue creates in the dimer was conducted using Discovery Studio 2.5 binding site analysis "Draw Ligand Interactions" tool and the hydrogen-bond and aromatic interactions monitors. Models of dimers (either WT/WT or with combinations of mutated structures) were minimized using 500 adopted basis Newton-Raphson method steps. Next the interactions created by specific residues were analyzed. Default values were used besides the cutoff distance of hydrogen-bond that was changed to 3.5 Å. The interactions that can be detected by this tool are aromatic-aromatic (π-π, sigma-π, cation-π), van der Waals (vdW), hydrogen-bond, charged interaction (electrostatic), and polar.

The data about mutations in 5-HT receptors were extracted from the GPCRDB (http://www.gpcr.org/7tm/) (Vroling et al., 2011).

Refinement of the Model

Docking. Protein-protein docking was done using the program HADDOCK (High Ambiguity Driven protein-protein DOCKing) (http://haddock.science.uu.nl/services/HADDOCK/haddock.php) (de Vries et al., 2010). HADDOCK is an information-driven flexible docking approach for the modeling of biomolecular complexes. For each docking run, the same monomer (either TRP_out2, TRP_in2, or TRP_out3) was uploaded to the HADDOCK "easy interface" server as molecules A and B. Residues Arg151$^{4.40}$, Arg152$^{4.41}$, Trp175$^{4.64}$, Arg176$^{4.65}$, and Tyr198$^{5.41}$ were defined as "active residues (directly involved in the interaction)." The numbers in superscript (4.40, 4.41, etc.) represent Ballesteros and Weinstein (1995) universal GPCR numbering, in which the most conserved position in TM X is denoted as X.50 and the other residues are numbered relative to it. All the HADDOCK solutions are clustered and ranked according to their HADDOCK scores. The HADDOCK score is the weighted sum of van der Waals, electrostatic, desolvation, and restraint violation energies, together with the buried surface area. As part of the scoring function (the "restraint violation energies"), HADDOCK performs a number of violation analyses, including the number of times a restraint is violated and the average distance and violation per restraint. As output, the best scoring structures of each cluster can be downloaded or directly viewed. Fast manual inspection of the models allowed filtering of nonrelevant models leaving only clusters of models in which the monomers are positioned correctly in the membrane. A representative of each resulting cluster of models was analyzed for the residues that contribute most to the interaction energy [by using the FastContact (Camacho and Zhang, 2005), COILCHECK (Alva et al., 2008), and Robetta alanine scan servers (Kortemme et al., 2004)]. Residues with $\Delta\Delta G > 2$ kCal were regarded as hotspots. The dimer interface was analyzed using the PROTORP server (http://www.bioinformatics.sussex.ac.uk/protorp/; Reynolds et al., 2009). PROTORP measures different interface physicochemical parameters such as the interface accessible surface area (interface size), the number of residues in the interface, the number of hydrogen bonds, gap index, and more (Reynolds et al., 2009).

Molecular Dynamics of WT and Mutant 5-HT$_{1A}$ Homodimers. We created mutant dimers by mutating several residues on one or both monomers of the HADDOCK out3-out3 dimer using the Discovery Studio mutagenesis tool.

These mutated dimers and the WT dimer were subjected to the leap Langevin simulated annealing refinement procedure in vacuum using the Chemistry at HARvard Macromolecular Mechanics (CHARMM) program (http://www.charmm.org/) (Brooks et al., 2009). The models underwent minimization of the 500 steepest-descent steps followed by 500 minimization adopted basis Newton-Raphson method steps before the simulated annealing. During the simulated annealing, the models were heated from 100 to 300 K and were left at 300 K for a production run of 15 ns (5-fs time step).

Root-mean-square deviation (RMSD) analysis of the TMs in the trajectories was done using the CHARMM Corrman RMS command. The TM definition was taken from the UniProtKB database (accession no. Q64264). Root-mean-square fluctuation per residue was calculated using the "rmsf-residue.str" CHARMM script created by Prof. Lennart Nilsson freely available at the script archive of the CHARMM forums. Residue RMSD per frame analysis was carried out using the VMD program (Humphrey et al., 1996) RMSD trajectory tool. Distance change during simulation was also calculated using VMD with a "distance.tcl" script from the VMD program script archive. All analyses were carried out on prealigned snapshots from the trajectories.

Defining 5-HT$_{1A}$ Putative Binding Site. We have defined the putative binding site of the 5-HT$_{1A}$ in two ways: 1) by using the ligand-docking results (Yap et al., 2012), which listed the residues that are in direct contact with serotonin (Ser199$^{5.42}$, Thr200$^{5.43}$, and Asp116$^{3.32}$) and pinolol (Asp116$^{3.32}$, Ile113$^{3.29}$, Lys191$^{5.34}$, and Asn386$^{7.39}$); 2) by using analogy to dopamine D$_3$ receptor (D3) X-ray structure. For this purpose, we superposed the 5-HT$_{1A}$ model

TRP_out3 onto chain A of the D3 X-ray structure PDB ID 3PBL (Chien et al., 2010). The superposition was carried out for the TM parts only, using Discovery Studio 2.5 superposition by sequence alignment tool. The alignment between the mouse 5-HT_{1A} and human D3 (accession no. P35462) and the definition of the TMs in 5-HT_{1A} were taken from UniProtKB. We extracted the residues that are in direct contact with the eticlopride in PDB ID 3PBL structure [Fig. 3 in (Chien et al., 2010)] and found the equivalent residues in 5-HT_{1A}. These were considered the second definition of the binding site of 5-HT_{1A} (Ala93$^{2.61}$, Asp110$^{3.32}$, Val111$^{3.33}$, Phe112$^{3.28}$, Cys114$^{3.36}$, Ile189, Thr196$^{5.39}$, Ser199$^{5.42}$, Thr200$^{5.43}$, Ala203$^{5.46}$, Trp342$^{6.48}$, Phe361$^{6.51}$, Phe362$^{6.52}$, Ala365$^{6.55}$, Leu366$^{6.56}$, Thr369$^{7.39}$, Gly382$^{7.35}$, and Tyr390$^{7.43}$).

Comparing the Putative 5-HT_{1A} Dimer with the μ-Opioid Receptor Dimer

We extracted the sequence of mouse μ-OR (accession no. P42866) and 5-HT_{1A} and aligned them using UniProt. For the μ-OR dimer, we have used the recently published structure PDB ID 4DKL. We used the protein interfaces, surfaces, and assemblies service PISA (Krissinel and Henrick, 2007) to reproduce the dimer that was reported in Manglik et al. (2012). Two 5-HT_{1A} TRP_out3 monomer copies were superimposed on both molecules of the μ-OR dimer using the Discovery Studio 2.5 package as described previously for the 5-HT_{1A} and the dopamine D_3 receptor. 5-HT_{1A} residues that are equivalent to the interface residues of the μ-OR dimer were extracted based on the structure-based sequence alignment.

Sequence Conservation Analysis

Sequences of 5-HT_{1A} from different species and of other 5-HT_1 receptor subtypes were extracted from the UniProtKB database (Supplemental Methods). Sequence alignments of the 5-HT_{1A} in different species and of mouse 5-HT_1 receptor subtypes were prepared using the alignment procedure of the UniProtKB server, which uses the ClustalW algorithm.

Results

Modeling of the 5-HT_{1A} Receptor Monomer. We used two servers, the M4T server (Fernandez-Fuentes et al., 2007) and the I-TASSER server (Roy et al., 2010) to construct several 3D models of the 5-HT_{1A} receptor, because no experimental structure of a monomer of 5-HT_{1A} or any other serotonin receptor is available. We repeated the modeling of the monomer, in the course of this work, as experimental structures continued to appear. The main difference between the different 5-HT_{1A} models is the location of residues Trp175$^{4.64}$ and Arg176$^{4.65}$. In some of the models (termed here TRP_in1, TRP_in2, etc.), Trp175$^{4.64}$ points into the TM bundle, whereas Arg176$^{4.65}$ points toward a potential dimeric interface (see Fig. 1, A and B). In other models, termed TRP_out1, TRP_out2, etc., Trp175$^{4.64}$ points out into the dimeric interface and Arg176$^{4.65}$ points into the TM bundle. Table 1 lists the monomers prepared for this study. For each monomer, the server that created it and the GPCR templates used for its preparation are shown. The models are similar to each other, with a TM backbone RMSD of 1.39 Å between models TRP_out1 and TRP_in1. The TM RMSD values are 1.25 Å between the M4T TRP_out1 and TRP_out2 models, 1.20 Å between the I-TASSER TRP_in1 and TRP_in2 models, and 1.68 Å between the TRP_in1 and TRP_out3 models. A unique feature of 5-HT_{1A} is that its IL3 is particularly long: it contains more than 100 residues (residue numbers 218–345) and is predicted to be partially disordered (see *Materials and Methods*). In experimentally determined GPCR structures, IL3 is either missing or replaced by the T4-lysozyme domain. Therefore, the IL3 loop of the 5-HT_{1A} receptor models is not expected to be reliably modeled and was shortened as described under *Materials and Methods*.

Modeling the 5-HT_{1A} Receptor Homodimers. Data from atomic force microscopy maps of rhodopsin in its native disk membrane was used for proposing a 3D molecular model of a GPCR oligomer (Fotiadis et al., 2003) This model showed an arrangement of rhodopsin molecules in two-dimensional arrays of dimers. In this arrangement, TM4, TM5, and IL2 (connecting TM3 and TM4) are involved in intradimeric interactions, whereas TM1, TM2, and IL3 (connecting TM5 and TM6) are involved in interdimeric interactions. We hypothesized that the dimeric organization in 5-HT_{1A} receptors is similar to that proposed for the rhodopsin (Liang et al., 2003; Niv and Filizola, 2008) and dopamine receptors (Guo et al., 2005).

The copies of the monomer models TRP_in and TRP_out were superposed on the structure of the rhodopsin dimer (chains A and C in PDB ID 1N3M). The corresponding resulting dimer models, in-dimer and out-dimer, were manually inspected and submitted to servers that estimate protein-protein interaction energies, such as COILCHECK (Alva et al., 2008) and FastContact (Camacho and Zhang, 2005). The residues that either contribute most to the interaction energy in the out-dimers [an example can be seen in (Supplemental Tables 1 and 2)] or that are potentially important for the dimerization based on manual inspection are Trp136$^{3.52}$ and Asp140$^{3.56}$ in IL2, Leu159$^{4.48}$, Leu166$^{4.55}$, and Trp175$^{4.64}$ in TM4 or in the beginning of EL2, and Tyr198$^{5.41}$ in TM5 (see Fig. 1A). Asp140$^{3.56}$ and Trp136$^{3.52}$ interact with Arg151$^{4.40}$, which has been shown to be important for signaling (Kushwaha et al., 2006).

In the TRP-in dimer, the residues that contribute most to the interaction are similar (Supplemental Tables 1 and 2): Trp136$^{3.52}$, Asp140$^{3.56}$, Leu166$^{4.55}$, and Tyr198$^{5.41}$. The main difference is that in the out-dimer Trp175$^{4.64}$ turns into the predicted dimeric interface, whereas in the in-dimer, Arg176$^{4.65}$ turns into the interface instead of Trp175$^{4.64}$ (as shown in Fig. 1, A and B). Consequently, Trp175$^{4.64}$ is predicted to contribute to the energy of the interactions in the out-dimers but not in the in-dimers. A representative structure of the out-dimer and the residues discussed above are shown schematically in Fig. 1C. Because both dimer models, TRP_in and TRP_out, are valid, both models were next used for suggesting mutations that may disrupt dimerization.

Design, Expression, and Glycosylation of Mutants in the Proposed Interface. On the basis of the 5-HT_{1A} homodimers model described above, mutations within the predicted interaction interface were designed to disrupt or weaken the dimerization interface (Table 2). The positive charge at the end of the TMs is important for correctly inserting the helix into the membrane (Lerch-Bader et al., 2008). Therefore, in residues Arg151$^{4.40}$, Arg152$^{4.41}$, and Arg176$^{4.65}$, we mutated the positively charged Arg into positively charged Lys, which is shorter and creates fewer interactions. In other cases, such as residues Trp136$^{3.52}$, Asp140$^{3.56}$, Leu159$^{4.48}$, and Leu166$^{4.55}$, we carried out the conventional mutagenesis into an Ala residue. Tyr198$^{5.41}$ was mutated to Phe, a minimal perturbation that can test the importance of hydrogen bonding at this position. Several

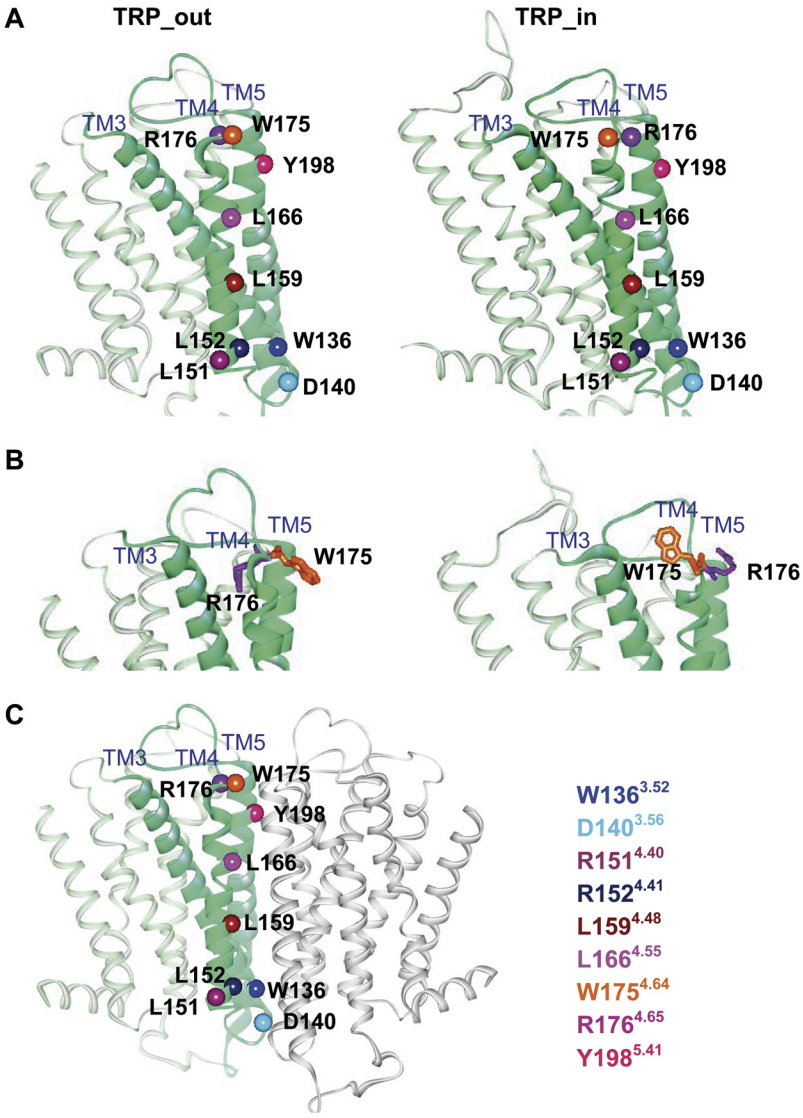

Fig. 1. A general model of 5-HT$_{1A}$ receptor monomer with residues predicted to participate in the dimer interaction interface. A, comparison between models TRP_out (left) and TRP_in (right). The monomers are shown as a cartoon green ribbon with emphasis on TM3, -4, and -5. The residues that are predicted to participate in the dimerization interface are represented as CPK (Corey-Pauling-Koltun space filling) model of their Cα atoms. These residues are positioned similarly along TMs 3 to 5, the only significant difference arising for Trp175$^{4.64}$ and Arg176$^{4.65}$; in TRP_out, Trp175$^{4.64}$ faces the interface, whereas Arg176$^{4.65}$ does not, and in TRP_in, this situation is exactly the opposite. B, a closer look at the difference between TRP_out (left) and TRP_in (right) monomers showing residues Trp175$^{4.64}$ and Arg176$^{4.65}$ in stick representation. C, a cartoon of the outdimer. The coloring of monomer I is the same as in A and B. Monomer II is depicted in gray.

TABLE 2
List of the 5-HT$_{1A}$ mutated constructs tested in this study and their cellular localization

Mutation	Region	Intracellular Localization
W136A/D140A	IL3	ER/Golgi
R151K/R152K	IL3	Plasma membrane
L159A/L166A	TM4	Plasma membrane
W175A	TM4-EL2	Plasma membrane
R176K	EL2	Plasma membrane
Y198F	TM5	Plasma membrane
W136A/D140A/R151K/R152K	IL3	ER/Golgi
R176K/Y198F	TM4 and TM5	Plasma membrane
R151K/R152K/Y198F	IL3 and TM5	ER/Golgi

mutations were combined to increase the potential effect of the construct on the dimerization.

To analyze the expression of substitution mutants, they were fused to different spectral variants of GFP and expressed in neuroblastoma N1E-115 cells, followed by SDS-PAGE and fluorescence analysis. Figure 2A demonstrates that the WT and all mutants were expressed at similar levels and were detectable as a double protein band. We hypothesized that the double bands shown in Fig. 2A for all constructs represent differently glycosylated receptor species. To test this hypothesis, the WT construct and the mutants were treated with PNGase-F, an enzyme that removes all types of N-linked carbohydrates. This treatment resulted in a single protein band shifted to approximately 55 kDa, as expected for the fusion construct, without any additional modifications, confirming that the two protein bands were indeed caused by different glycosylation (Fig. 2B). Treatment of probes with EndoH, which removes only carbohydrates of the high mannose type, revealed that the upper protein band is not shifted and hence contains processed carbohydrates. In contrast, the lower species shift to the same position as the PNGase-F-treated protein and therefore contain unprocessed carbohydrates of the high mannose type (Fig. 2B). Attachment of unprocessed carbohydrates of the high mannose type occurs in the endoplasmic reticulum (ER), whereas terminal glycosylation takes place in the trans-Golgi and represents an important signal for transporting receptors to the plasma membrane.

To characterize a precursor-product relationship for various receptor mutants, the intensities of the upper (processed) and the lower (unprocessed) protein bands were compared. As shown in Fig. 2C, the upper/lower band ratio for the W175A, R176K, Y198F, L159A/L166A and R176K/Y198F

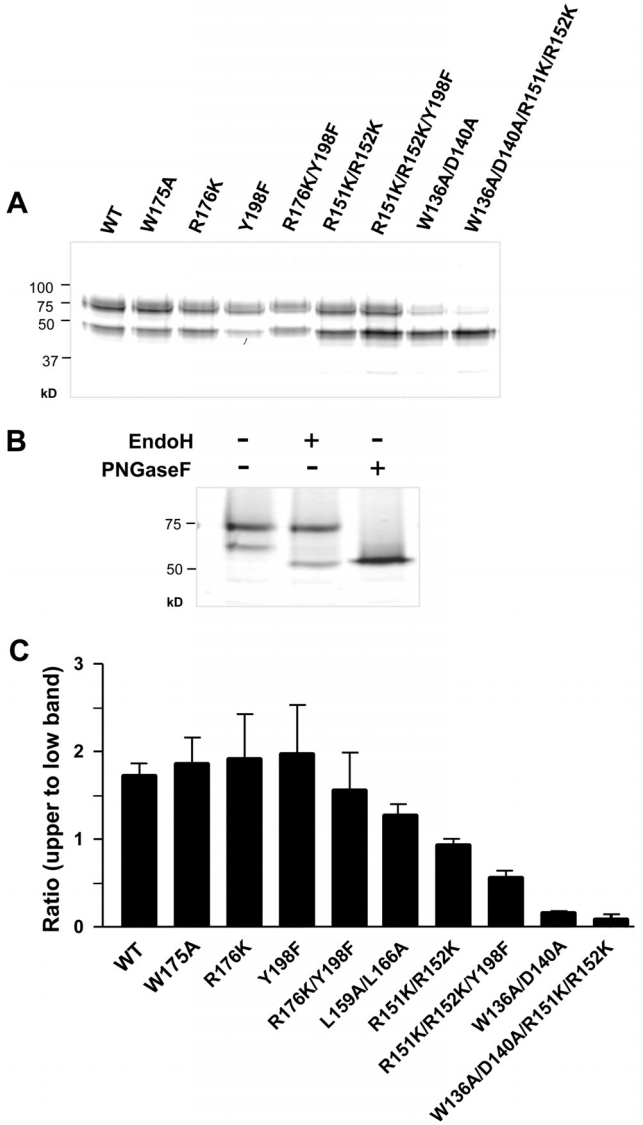

Fig. 2. Expression and glycosylation of 5-HT_{1A} receptor wild-type and substitution mutants. A, analysis of different YFP-tagged 5-HT_{1A} receptor constructs transiently expressed in neuroblastoma N1E-115 cells. The SDS-PAGE gel was scanned at λ_{ex}488 nm, and emission was collected by using a band pass filter 530/25. The molecular mass marker is indicated on the left. B, the 5-HT_{1A} receptor was digested with EndoH or PNGase-F or was left untreated before SDS-PAGE and detection. Representative scans for 5-HT_{1A} receptor WT are shown. C, the precursor-product relationship of the WT and mutants plotted as the intensity ratio of the upper to the lower protein bands that are shown in A. Data points represent the means ± S.E.M. from at least three independent experiments.

mutants was similar to that obtained for the WT receptor, suggesting their correct processing and transport to the plasma membrane. The ratio was slightly decreased with the R151K/R152K mutant [suggesting that this mutant had higher retention in the ER, as was predicted for several mutations in Arg151 including R151K (Kushwaha et al., 2006)]. In contrast, the ratio was significantly decreased in the R151K/R152K/Y198F, W136A/D140A, and W136A/D140A/R151K/R152K mutants, suggesting their predominant localization in the ER. Taken together, these results indicate that most, but not all, of the 5-HT_{1A} receptor mutants undergo complete processing and can therefore be targeted to the cytoplasmic membrane.

Subcellular Distribution of Mutant. We next analyzed the subcellular distribution of mutants to detect their exact localization in the cells. Confocal microscopy performed after transfection of WT 5-HT_{1A}-YFP constructs into N1E-115 cells indicated that most of the receptors were present on the plasma membranes and only a minor fraction of them was present in the intracellular compartments (Fig. 3). For the W175A, R176K, Y198F, R176K/Y198F, L159A/L166A, and R151K/R152K mutants, we obtained a similar distribution, which is also consistent with the glycosylation data (Fig. 2C). In contrast, the membrane localization was lost for the R151K/R152K/Y198F, W136A/D140A, and W136A/D140A/R151K/R152K mutants, and these proteins were homogeneously distributed within the cytoplasm (Fig. 2C; Table 2). These combined data indicate that the W175A, R176K, Y198F, R176K/Y198F, L159A/L166A, and R151K/R152K mutants possess biochemical features as well as subcellular distributions similar to the WT 5-HT_{1A} receptor, whereas others have modified distributions.

Modified cellular distribution of GPCR mutants is a well documented phenomenon, which may occur naturally, sometimes causing pathologic conditions (Pulagam and Palczewski, 2010), or in site-directed mutagenesis (Milligan, 2009). We return to this issue under *Discussion*, whereas the rest of this work focuses on mutants that localize at the plasma membrane: W175A, R176K, Y198F, R151K/R152K, L159A/L166A, and R176K/Y198F.

Pharmacological Analysis of Mutants. Having demonstrated the plasma membrane localization of W175A, R176K, Y198F, R151K/R152K, L159A/L166A, and R176K/Y198F mutants, we next analyzed whether their pharmacological properties are affected. Pharmacological profiling of the wild-type and mutated receptors by competitive binding of the radioactively labeled agonist [^{3}H]8-OH-DPAT and nonradioactive 8-OH-DPAT revealed no significant differences among the receptor constructs (Fig. 4). The IC_{50} values calculated for mutants were also similar to the IC_{50} WT 5-HT_{1A} receptor (Table 3). These results are in line with the predicted ligand-binding site, which was not expected to be affected by the mutation (Supplemental Fig. 1). It is noteworthy that the pharmacological results obtained in the present study are in line with published data on the recombinant 5-HT_{1A} receptor in membrane preparations of Chinese hamster ovary cells, where a logIC_{50} value of −8.42 ± 0.06 for the wild type receptor was calculated (Khawaja et al., 1997). Thus, all membrane-localized mutants possess the same pharmacological properties as the 5-HT_{1A} receptor wild type.

Analysis of 5-HT_{1A} Receptor Oligomerization by Using Acceptor Photobleaching FRET. We have recently established a confocal microscopy-based acceptor photobleaching FRET assay to demonstrate the oligomerization of the 5-HT_{1A} receptor at the single-cell level (Kobe et al., 2008). In the present study, this method was applied to compare the oligomerization efficiency of the WT and the five plasma membrane-localized mutants that were designed to have impaired receptor oligomerization. Neuroblastoma N1E-115 cells were transfected with 5-HT_{1A}-CFP (donor) and 5-HT_{1A}-YFP (acceptor) fusion constructs in different combinations, and receptors expressed in the plasma membrane (Fig. 5A) were analyzed for interaction. To avoid artifacts resulting from overexpression, we adjusted the total expression level

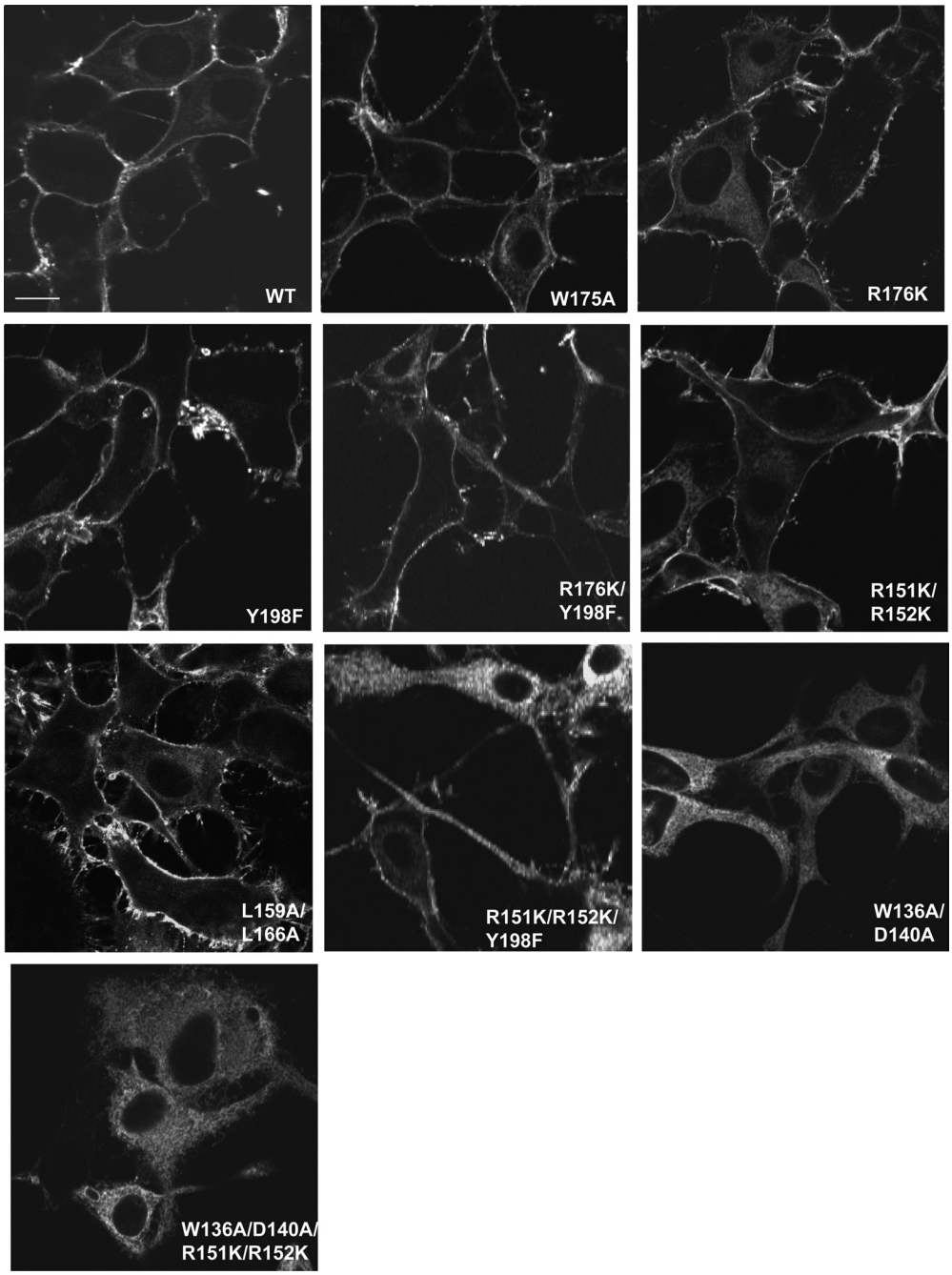

Fig. 3. Subcellular distribution of the 5-HT$_{1A}$ receptor wild-type and mutants. Representative confocal images of YFP-tagged receptors obtained with a LSM780-Meta microscope at 63× magnification are shown. Scale bar, 10 μm.

for the CFP- and YFP-tagged receptor to 1.0 to 1.2 fmol/mg proteins in all the following FRET experiments, which allows for quantitative analysis of results obtained in different experiments. Moreover, a similar amount of endogenous 5-HT$_{1A}$ receptors was obtained in the hippocampus under physiological conditions (Hoyer et al., 1986).

Figure 5B shows the bleached region of interest with a loss of YFP intensity as well as a reference region of interest from which the acquisition bleaching rate was determined for corrected FRET calculation. In the bleached region of interest, the loss of acceptor fluorescence was accompanied by increased donor emission intensity that is characteristic of FRET. In contrast, the intensities of both CFP and YFP fluorescence in nonbleached regions undergo only minor decreases (acquisition bleaching).

Finally, the apparent FRET efficiency, Ef_D, was calculated (eqs. 1 and 2). Data were background-subtracted and corrected for acquisition bleaching using the measurements from the reference region of the plasma membrane (Fig. 5C). The WT receptor fusion proteins from cells with similar donor-to-acceptor (CFP-to-YFP) ratios were found to have a mean apparent FRET efficiency of 18.9 ± 0.6%, which is in accordance with our previous results (Kobe et al., 2008). After expression of CFP- and YFP-tagged W175A and R151K/R152K mutants, FRET efficiency was significantly reduced to 12 ± 0.7 and 11.9 ± 0.6%, respectively. In addition, coexpression of W175A with either the R176K or Y198F mutants resulted in a decrease of FRET signal to 12 ± 0.7 and 13 ± 1%, respectively. Double-mutant R176K/Y198F presented on both monomers reduces the FRET efficiency to

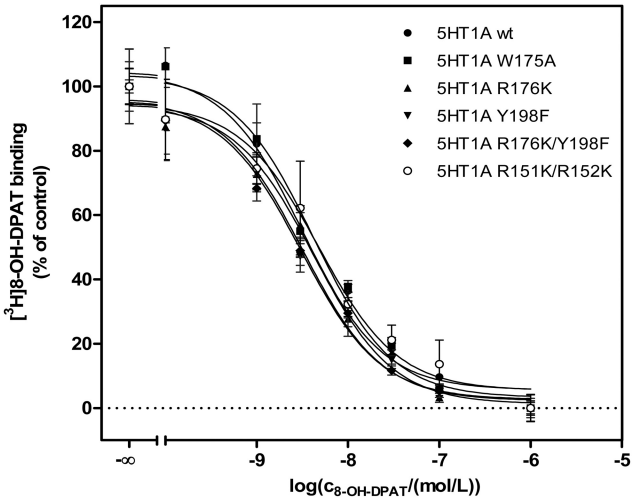

Fig. 4. [^{3}H]8-OH-DPAT competition binding at various 5-HT$_{1A}$ receptor mutants. Membranes of N1E-115 cells expressing either wild-type or plasma membrane localized 5-HT$_{1A}$ receptor mutants (18 μg of total protein) were subjected to the competition binding by incubation with 1 nM [^{3}H]8-OH-DPAT along with increasing concentrations of nonradioactive 8-OH-DPAT. Data are shown as mean ± S.D. Data were analyzed by nonlinear regression and fitted to monophasic competition isotherms.

TABLE 3

LogIC$_{50}$ values of [^{3}H]8-OH-DPAT competition binding at various 5HT$_{1A}$ receptor mutants

Data shown in Fig. 4 were analyzed by nonlinear regression and fitted to monophasic competition isotherms to obtain logIC$_{50}$ values ± S.D. for 8-OH-DPAT for each receptor mutant. Pairwise comparison of the Gaussian-distributed logIC$_{50}$ values using one-way analysis of variance followed by Bonferroni's t test showed no significant differences between the wild-type and all mutants tested.

5HT1A Receptor Mutation	logIC$_{50}$ ± S.D.	IC$_{50}$ (95% CI)
		nM
Wild-type	−8.50 ± 0.07	3.18 (2.23–4.53)
W175A	−8.38 ± 0.06	4.14 (3.04–5.63)
R176K	−8.38 ± 0.06	4.17 (3.22–5.40)
Y198F	−8.50 ± 0.06	3.19 (2.34–4.35)
R176K/Y198F	−8.51 ± 0.07	3.06 (2.23–4.20)
R151K/R152K	−8.32 ± 0.10	4.77 (2.96–7.69)

CI, confidence interval.

13.5 ± 1.3%. In contrast, FRET efficiency was not changed when R176K-CFP and R176K-YFP or Y198F-CFP and Y198F-YFP combinations were analyzed. Likewise, combining WT with either W175A, Y198F, or R176K mutants, as well as coexpression of R176K with Y198F or W175A with R151K/R152K did not influence the FRET efficiency (Fig. 5C).

These data suggest that Trp175$^{4.64}$ residues from different monomers are involved in forming the interaction interface. Trp175$^{4.64}$ can also interact with Arg176$^{4.65}$ and Tyr198$^{5.41}$ located on the opposite monomer to stabilize the receptor complex. In addition, interactions of both Arg176$^{4.65}$ and Tyr198$^{5.41}$ with Arg176$^{4.65}$ and Tyr198$^{5.41}$ residues on the opposite monomer may contribute to dimerization, even though a single mutation is not enough to disrupt it. These results provide a stronger support to the TRP_out models than the TRP_in model (Fig. 1). Another important region of dimerization is likely to be formed by residues Arg151$^{4.40}$ and Arg152$^{4.41}$, which can interact with the corresponding amino acids on the opposite monomer.

No decrease in dimerization was found for combinations of either WT or mutant constructs with the L159A/L166A mutant. These results indicate that Leu159$^{4.48}$ and Leu166$^{4.55}$ are probably not pivotal for maintaining the binding interaction between the two 5-HT$_{1A}$ monomers.

Analysis of 5-HT$_{1A}$ Receptor Dimerization by the Lux-FRET. The apparent FRET efficiency, Ef_D, measured by the acceptor photobleaching is inherently dependent on f_D, the fraction of donor participating in FRET complexes. This is in turn dependent upon the ratio of total donor concentration [D_t] to total acceptor concentration [A_t] present in the sample. It has been suggested that the dependence of Ef_D on [A_t]/[D_t] may be useful in differentiating FRET resulting from specific versus random interactions (James et al., 2006). In the case of random interaction, Ef_D has been predicted to be independent of the total donor-to-acceptor ratio at a fixed surface density above a certain ratio. Therefore, we next calculated the apparent FRET efficiencies for donors, Ef_D, and acceptors, Ef_A, over a wide range of donor molar fraction, x_D [$x_D = [D^t]/([D^t]+[A^t])$]. For that we applied quantitative linear unmixing FRET (lux-FRET) method, which allows determination of all aforementioned parameters (Wlodarczyk et al., 2008). Using the lux-FRET approach, we have previously demonstrated the specificity of 5-HT$_{1A}$ receptor oligomerization (Kobe et al., 2008; Woehler et al., 2009) and performed detailed analysis of the 5-HT$_{1A}$ oligomerization behavior in living cells (Renner et al., 2012). In the present study, we applied the lux-FRET method to quantify apparent FRET efficiency as a function of donor/acceptor ratio for wild-type and mutated 5-HT$_{1A}$ receptors. To be able to perform quantitative comparison of FRET values obtained at different donor-to-acceptor ratios, the total concentration of plasmids encoding for donor and acceptor was held constant in all experiments. Graphs shown in Fig. 6 clearly demonstrate functional dependence of both Ef_D and Ef_A from the donor molar fraction, x_D, thus confirming specific receptor-receptor interaction. Based on the lux-FRET analysis, we also estimated the number of units participating in complex, n (eqs. 3 and 4) and obtained a best fit for the value of $n = 2.2$ ($R^2 = 0.94$; Fig. 6A) for the 5-HT$_{1A}$ receptor wild-type. The goodness of fit was similar in the range from $n = 2.1$ to $n = 2.3$ (Supplemental Fig. 2). After coexpression of the WT-YFP (acceptor) with W175A-CFP (donor), the n values reside at a similar range ($n = 2.0$, $R^2 = 0.97$; Fig. 6B), and the maximal R^2 values obtained for n ranged from 1.9 to 2.1 (Supplemental Fig. 2). In contrast, after coexpression of W175A-CFP with W175A-YFP n-value was lowered to $n = 1.4$ ($R^2 = 0.95$; Fig. 6C and Supplemental Fig. 2). The coexpression of W175A-CFP (donor) with Y198F-YFP (acceptor) also resulted in decreasing the n value, to n ranged from 1.3 to 1.5 ($R^2 = 0.90$; Supplemental Fig. 2). These results indicate that amount of receptors existing in monomeric form was increased after expression of the W175A mutant or after coexpression of W175A with Y198F mutant, compared with the WT receptors (expressed alone or in combination with W175A). Taken together, these data confirm the importance of amino acids Trp175$^{4.64}$ and Tyr198$^{5.41}$ in forming the dimeric complex.

Refinement of the Model. Anchor-driven simulated annealing molecular dynamics was successfully used to predict peptide interactions with homology models of postsynaptic density 95/discs-large/zona occludens (PDZ) domains (Niv and Weinstein, 2005) and to incorporate experimental constraints into an activated model of rhodopsin (Niv et al.,

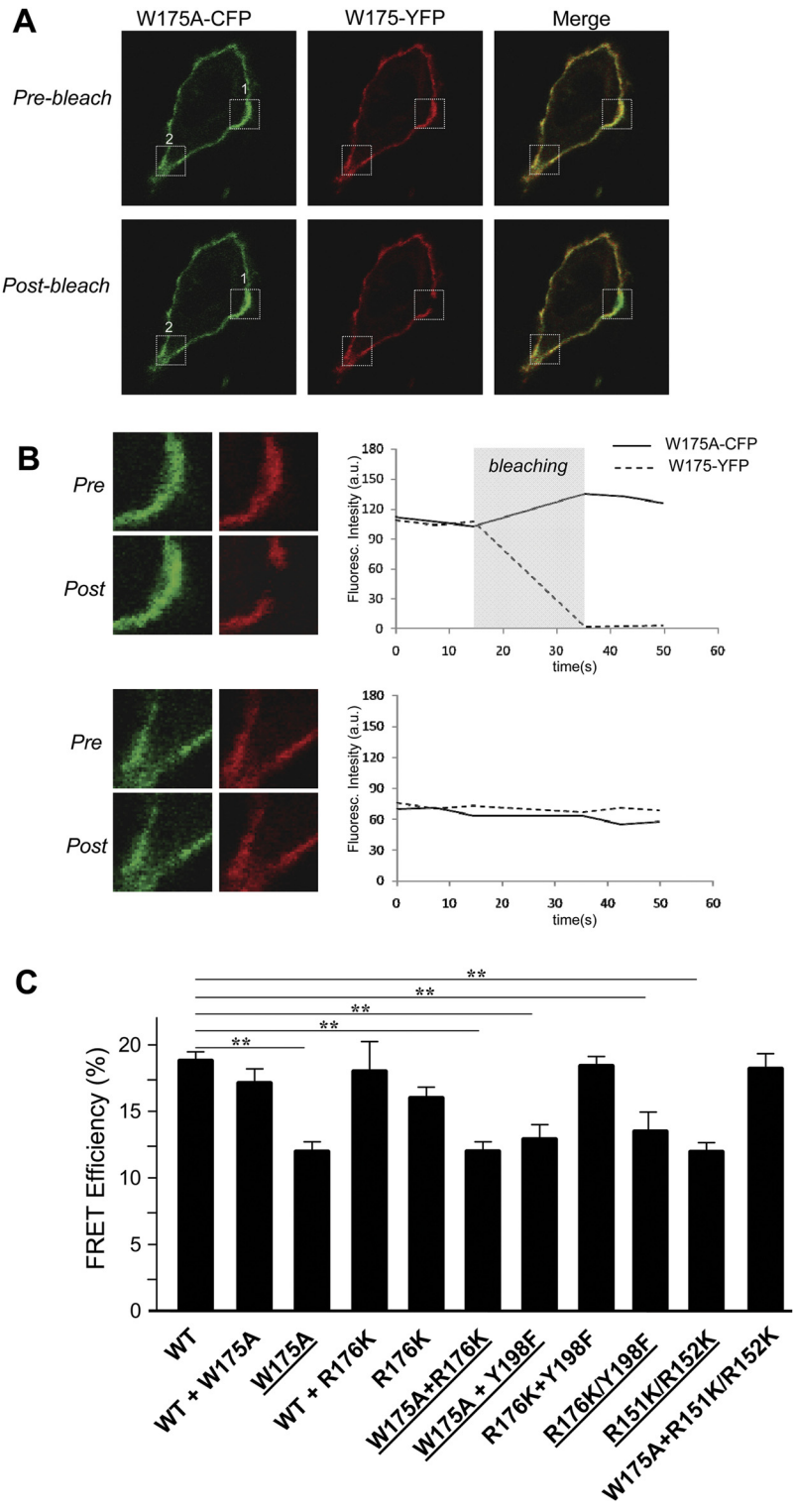

Fig. 5. Acceptor photobleaching FRET analysis of 5-HT$_{1A}$ receptor dimerization. A, confocal microscopy was used to visualize 5-HT$_{1A}$-CFP and 5-HT$_{1A}$-YFP coexpressed in the plasma membrane of N1E-115 cells. Fluorescence spectra were collected and unmixed for CFP and YFP components using the Zeiss LSM780-Meta detector. The fluorescence image of the CFP channel (green), the YFP channel (red), and composite channel before and after bleaching are shown. Box 1 corresponds to the bleached regions of interest, whereas box 2 corresponds to the nonbleached regions of interest. Scale bar, 10 μm. B, enlargement of box 1 is shown at the top left. The 12-bit grayscale intensities of YFP and CFP during the whole trial are plotted for the bleached regions of interest (right). Enlargement of box 2 is shown at bottom left. The 12-bit grayscale intensities of YFP and CFP during the whole trial are plotted for the nonbleached regions of interest (right). C, the apparent FRET efficiency, Ef_D, was calculated according to eqs. 1 and 2. Data are shown as mean ± S.E.M. **, $p < 0.01$. Mutations with significantly reduced Ef_D values are underlined.

2006). Here we used the restraints-driven protein-protein docking tool HADDOCK (de Vries et al., 2010) to dock two protomer copies of either TRP_out2, TRP_in2, or TRP_out3, using constraints as described below.

The results of our experimental procedures indicated that the W175A mutation decreases oligomerization when placed in both (but not in a single) monomers. R176K placed in both monomers does not influence dimerization, but the combination of R176K in one monomer with W175A in the other monomer decreases dimerization. This suggests interaction between Trp175$^{4.64}$ and Arg176$^{4.65}$. Mutant Y198F alone or in combination with R176K does not influence dimerization, but W175A in combination with Y198F reduces dimerization. This suggests the existence of interaction between Trp175$^{4.64}$ and Tyr198$^{5.41}$.

In summary, our experimental results indicate interactions between Trp175$^{4.64}$ in one monomer with Trp175$^{4.64}$, Arg176$^{4.65}$, and Tyr198$^{5.41}$ in the other monomer, possibly

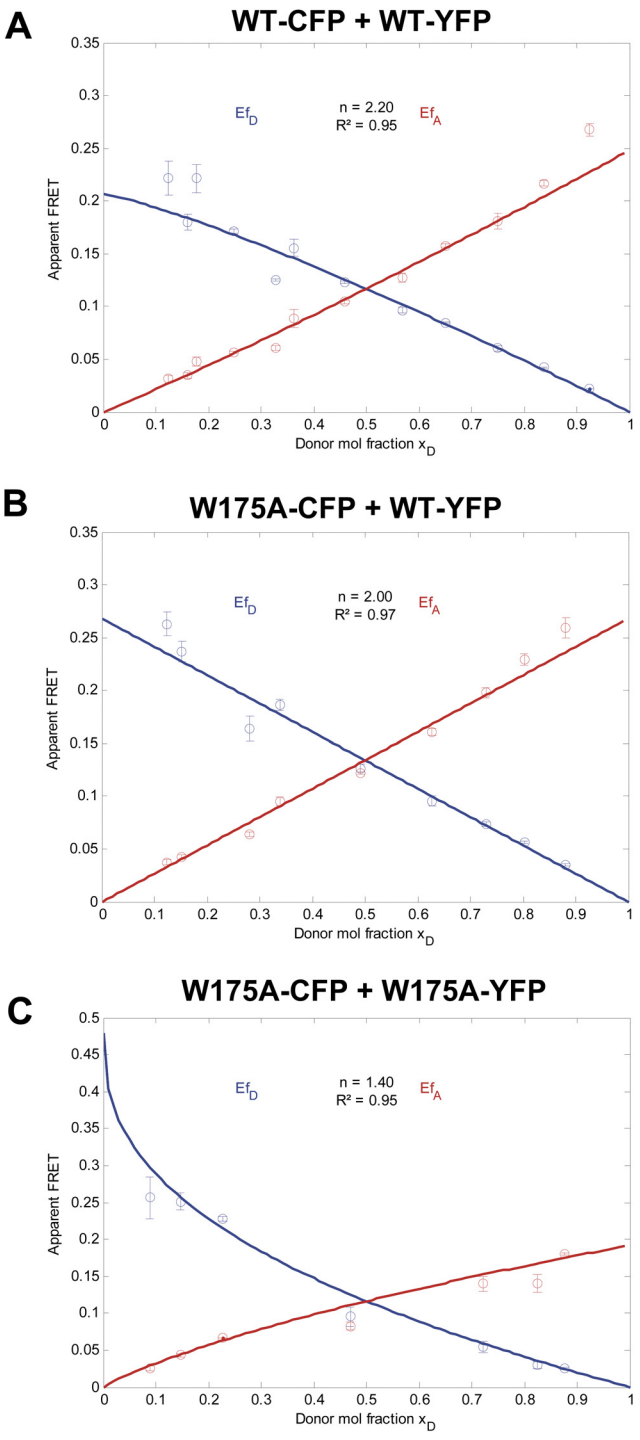

Fig. 6. Oligomerization of 5-HT_{1A} receptor wild type and mutants investigated by the lux-FRET. Apparent FRET efficiencies Ef_D (blue) and Ef_A (red) were calculated according to Wlodarczyk et al. (2008) and are shown as functions of the donor mole fraction x_D for the wild-type homomers (A), wild-type/W175A heteromers (B), as well as for the W175A homomers (C). Experimental data were fitted according to eqs. 3 and 4, where n represents a number of units participating in complex. Data points represent the mean ± S.E.M. of the apparent FRET efficiency values from at least three independent experiments.

simultaneously. In addition, mutations R151K/R152K placed in both monomers decrease dimerization.

The residues $Arg151^{4.40}$, $Arg152^{4.41}$, $Trp175^{4.64}$, $Arg176^{4.65}$, and $Tyr198^{5.41}$ were used as constraints in HADDOCK (de Vries et al., 2010) by defining them as "active residues" (residues directly involved in the interaction). A default docking run resulted in up to 200 refined putative solutions. These solutions were clustered based on their structural similarity, as measured by RMSD (clustering details described under *Materials and Methods*). Parameters for representative models in each cluster, such as the HADDOCK energy score and its components (van der Waals energy, electrostatic energy, desolvation energy, and the penalty energy due to violation of restraints), the number of models in the cluster, and the interface size [the buried surface area (square Ångstroms) in both monomers] were reported (Table 4).

TABLE 4
HADDOCK scoring and evaluation of the in2-in2 and out3-out3 dimers suggest that out3-out3 is preferable to in2-in2 model
HADDOCK final score, the size of the cluster, the average backbone RMSD from the lowest energy structure of the cluster, van der Waals, electrostatic and desolvation energies and the buried surface area in the dimer are shown for top cluster of two models.

Parameter	in2-in2 dimer	out3-out3 dimer
Monomer	TRP_in2	TRP_out3
HADDOCK score	−118.7 ± 3.1	−239.5 ± 5.7
Cluster size	55	200
RMSD from the overall lowest-energy structure in the cluster, Å	29.0 ± 0.9	1.1 ± 0.8
van der Waals energy, kcal/mol	−46.5 ± 3.2	−93.0 ± 10.1
Electrostatic energy, kcal/mol	−14.7 ± 21.2	−73.0 ± 20.5
Desolvation energy, kcal/mol	−69.3 ± 9.1	−136.7 ± 8.9
Restraint violation energy	1.0 ± 1.00	48.2 ± 13.28
Buried surface area, $Å^2$	1604.1 ± 235.7	2859.6 ± 103.4

Representative structures in the resulting clusters of docking solutions were inspected manually for the general positioning of the monomers with respect to each other and to the membrane. In the docking solutions of TRP_out2 monomers, no representative models passed the manual inspection and were not analyzed further. For docking solutions of TRP_in2 monomers (termed in2-in2), the first cluster of the docked models contained 55 structures, from which a representative, well behaved model was obtained. In the rest of the clusters, the monomers were not positioned well with respect to each other and to the membrane. The docking solutions of the TRP_out3 monomer resulted in one cluster, consisting of all of the 200 models. The parameters for the top-ranked structure in each cluster are presented in Table 4.

To compare these refined, constraint-driven models (in2-in2 and out3-out3) with the preliminary models that we obtained by superimposing the monomers on a PDB ID 1N3M template (TRP_out2-dimer, TRP_in2-dimer, and TRP_out3-dimer; Fig. 1), we assessed the models using PROTORP server (Reynolds et al., 2009). PROTORP is a bioinformatics tool designed to analyze the interfaces between soluble protein chains in protein-protein complexes by calculating a set of physicochemical parameters exhibited by each protein interface. To the best of our knowledge, no analogous analysis has yet been done in membrane proteins. With this caveat in mind, Table 5 presents part of the interface properties that were measured. These measures are commonly used for identifying true versus false interfaces. For example, the average interface area per monomer calculated for 122 homodimers was found to be 1940 $Å^2$, the average number of residues in the interface was 52, and the average number of hydrogen-bonds was 9 (Bahadur et al., 2003). In addition, the monomers in real interfaces usually have good complementarity. One way to evaluate the complementarity of the monomers in

TABLE 5
PROTORP values for interface parameters in different 5-HT$_{1A}$ dimer models suggest the out3-out3 as the optimal model

	TRP_out2-Dimer	TRP_in2-Dimer	TRP_out3-Dimer	HADDOCK in2-in2	HADDOCK out3-out3
Monomer	TRP_out2	TRP_in2	TRP_out3	TRP_in2	TRP_out3
Interface area on one monomer, Å^2	475.10	654.74	325.64	814.40	1478.17
Number of residues	19	19	18	23	37
Interactions (hydrogen-bonds and electrostatic)	6	4	0	12	11
Gap index				4.72	1.59

the interface is the gap index. A lower gap index indicates higher complementarity (Jones and Thornton, 1996). Judging by their larger interface, with a higher number of residues in the interface, and a higher number of hydrogen or electrostatic contacts, the monomers are positioned better in the refined HADDOCK models than in the preliminary PDB ID 1N3M-based models. In silico alanine scanning, using the Robetta alanine scan server (Kortemme et al., 2004), was performed as an additional evaluation measure. No hotspots were predicted in any of the preliminary dimers, whereas for the refined models, the Robetta server predicted both Trp175$^{4.64}$ and Tyr198$^{5.41}$ to be hotspots. Between the two HADDOCK models, the out3-out3 dimer has better values both in its HADDOCK cluster parameters (Table 4) and in most PROTORP parameter values (Table 5). For example, the cluster that includes the best putative model is significantly larger and the HADDOCK score for the top-ranking model is better; this model's interface size approaches the average homodimers' interface sizes, and it has a higher number of residues in the interface. The number of interactions is similar for the two models (Table 4), but the HADDOCK out3-out3 dimer has fewer gaps than does the HADDOCK in2-in2 dimer.

The superior quality of the out3-out3 model is in accord with the experimental results mentioned earlier, which indicated that Trp175$^{4.64}$ is located at the interface, as is the case in the out3-out3 but not in the in2-in2 dimer. Based on these combined data, out3-out3 was chosen as the best current model of the dimer. Figure 7A gives a general overview of the out3_out3 dimer.

Rationalizing the Data Obtained for the Receptor Mutants. Several combinations of mutations were experimentally shown to decrease the dimerization. It is noteworthy that a mutation on only one of the monomers did not significantly reduce the dimerization. This indicates that mutants were still capable of maintaining strong interactions with the WT. We aimed at understanding the detailed structural and molecular reasons underlying these observations. The fine-tuned HADDOCK out3-out3 dimer now enables such a detailed analysis of the interactions in the interface (Fig. 7, B and C).

We analyzed the contacts created by residues Trp175$^{4.64}$ and Tyr198$^{5.41}$ using the WT dimer and the mutant dimers (Supplemental Table 3). In the WT dimer, residue Trp175$^{4.64}$ of both monomers creates aromatic-aromatic (π-π) interactions with each other. In addition each of them [Trp175$^{4.64}$ on monomer I (I:Trp175) and Trp175$^{4.64}$ on monomer II (II:Trp175)] is involved in vdW interactions with Tyr198$^{5.41}$ on the opposite monomer [Fig. 7C and (Supplemental Table 3)]. Trp175$^{4.64}$ on both molecules is indeed predicted to be the strongest hotspot in the Robetta alanine scan (Kortemme et al., 2004). It is therefore not surprising that when Trp175$^{4.64}$ is mutated in both monomers, the dimerization decreases significantly. The analysis of the contacts also reveals that no contacts are made by the mutated W175A residues. It is noteworthy that when only one Trp175$^{4.64}$ is mutated, the dimerization ability is only marginally lowered (Fig. 5C). This can be explained by the fact that in the WT/W175A dimer model, the vdW interaction still exists between the mutant W175A and WT Trp175$^{4.64}$. Alternatively, Trp175$^{4.64}$ on the WT monomer can still interact with Tyr198$^{5.41}$ of the mutated monomer, which, in turn, can move to create even stronger interactions with Tyr198$^{5.41}$.

The Tyr198$^{5.41}$ residue was also predicted to be a hotspot by the alanine-scan. Indeed, in the WT out3-out3 dimer model, Tyr198$^{5.41}$ is involved in several interactions, including hydrogen-bond between the OH groups of the I:Tyr198 and II:Tyr198 and interaction with Trp175$^{4.64}$ in the opposite monomer (Fig. 7C). When Tyr198$^{5.41}$ is mutated to Phe in one monomer, it loses the hydrogen bond with the Tyr198 on the opposite monomer, but it can still create most of the WT interactions. However, when Trp175$^{4.64}$ is mutated to Ala in monomer I (I:W175A) and Tyr198$^{5.41}$ to Phe in monomer II (II:Y198F), the interface loses both the aromatic interaction between I:Trp175 and II:Trp175 and the hydrogen bond between the Tyr198$^{5.41}$ residues. In addition, the mutated residues W175A and Y198F cannot create compensating interactions in the way that Tyr198 and Trp175 probably do in the WT/W175A and W175A/WT combinations. We deduce that the aromatic interactions created by I:Trp175 with II:Trp175, the interaction between Trp175$^{4.64}$ and Tyr198$^{5.41}$ on opposite monomers, and the hydrogen bond between I:Tyr198 and II:Tyr198 (Fig. 7C; Supplemental Table 3) have a pivotal effect on the total interaction energy of the dimerization. The interactions involving Arg151$^{4.40}$ and Arg152$^{4.41}$ in our model are not strong enough to explain their pivotal role in the interface, as seen in the FRET experiments (Supplemental Table 3).

To further investigate the role of Arg151$^{4.40}$ and Arg152$^{4.41}$ in dimerization, specific interacting residues should be identified. Our models suggested that they may interact with residues from IL2 in the other monomer, such as Trp136 $^{3.52}$ and Asp140$^{3.56}$. However, W136A/D140A double-mutant 5-HT$_{1A}$ constructs did not reach the plasma membrane (Figs. 2 and 3; Table 2), and therefore we could not test this hypothesis. The refined 5-HT$_{1A}$ models suggest an additional residue, Asp143$^{3.59}$, as a candidate for interacting with Arg151$^{4.40}$ and Arg152$^{4.41}$. The refined model not only predicts Asp143$^{3.59}$ to be in the interface but it also suggests that this residue may have high contribution to the binding energy.

Using the initial computational dimer model we have predicted several residues on the surface of 5-HT$_{1A}$ to be important for 5-HT$_{1A}$ dimerization. The experimental procedures have shown that indeed some of these residues are pivotal for

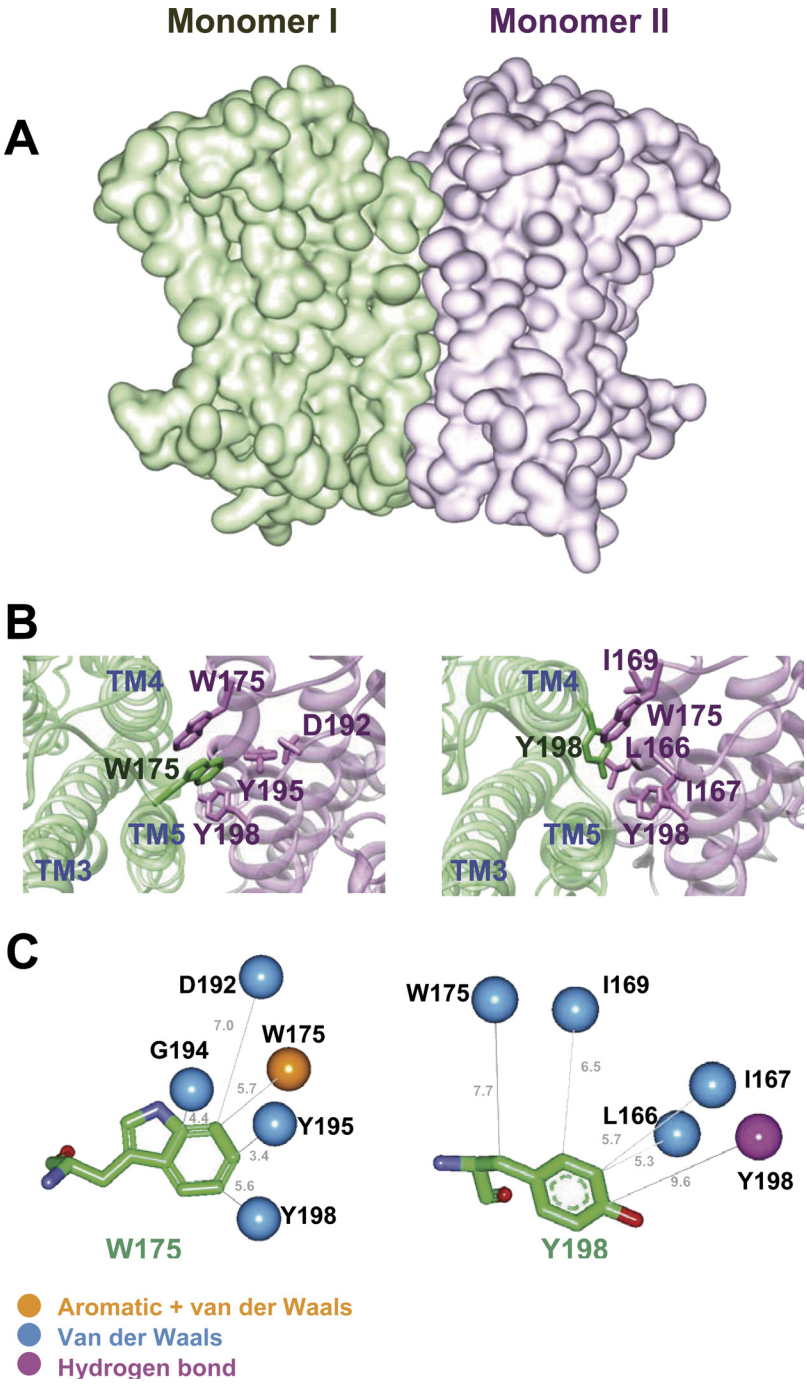

Fig. 7. The dimer and interface interactions in the HADDOCK out3-out3 dimer. A, good complementarity between the monomers in the HADDOCK out3_out3-dimer. The monomers are shown in surface representation. Monomer I is shown in green and II in purple. The interface between the monomers is large and continuous (without many gaps). B, a top 3D view of residues I:Trp175$^{4.64}$ (left) and I:Tyr198$^{5.41}$ (right) and the residues from monomer II that interact with them are shown. The residues are shown in green stick representation for monomer I and in purple stick representation for monomer II. Monomer I is shown in green and II in purple, both are shown as ribbons. C, a cartoon representation of the residue I:Trp175$^{4.64}$ (left) and I:Tyr198$^{5.41}$ (right) and their interacting residues in molecule II. I:Trp175$^{4.64}$ and I:Tyr198$^{5.41}$ are shown in stick representation. The carbon atoms are in green, oxygen in red, and nitrogen in light purple. The interacting residues from monomer II are represented by their Cα atoms as colored spheres, and their colors represent the interaction type with the color coding marked in the figure outline. The distances (in Ångstroms) between the Cα atoms of the residues in monomer II and the closest carbon atom in either Trp175$^{4.64}$ or Tyr198$^{5.41}$ are shown in gray.

the dimerization, and these data allowed fine-tuning of the 5-HT$_{1A}$ homodimer model. The resulting fine-tuned 5-HT$_{1A}$ homodimer model provides detailed information about these interactions.

To evaluate the robustness of our conclusions, we subjected the WT HADDOCK out3-out3 dimer and several combinations of mutants (WT with II:W175A, I:W175A with II:W175A, WT with II:Y198F and I:Y198F with II:W175A) to 15 ns of MD simulation. To see the effect of a more pronounced mutation in residue Tyr198$^{5.41}$, we also carried out an MD simulation of the WT/II:Y198A combination, although this mutation was not generated experimentally. The trajectories were analyzed with focus on the behavior of residues 175$^{4.64}$, 176$^{4.65}$, and 198$^{5.41}$ on both monomers. The overall stability of the monomers and the dimers was examined by manual inspection and TMs Cα RMSD monitoring during the run analysis. In five of six unrelated WT/WT runs, the overall structure of the monomers and dimers remained stable during the simulation. The average RMSD of the TMs stabilized after a few nanoseconds (Supplemental Fig. 3). Residue root-mean-square fluctuation analysis also suggested that the structures are stable (data not shown).

In the WT/II:Y198A MD simulation the RMSD of the TM Cα increases throughout the simulation as opposed to the TM Cα RMSD of the WT/Y198F. It is noteworthy that the change is due to one of the monomers' tilting with respect to the other monomer and to the membrane. Because such a change is not feasible within a realistic membrane, this may suggest

that in the realistic membrane the stability of this dimer is reduced compared with the WT.

We obtained decreased dimerization in W175A/W175A and W175A/Y198F combinations of mutants, whereas the combination WT/W175A did not impair the dimerization. We hypothesized that in the WT/W175A combination the remaining I:Trp175 that cannot interact with the mutated II:W175A may strengthen its interaction with II:Tyr198, whereas II:Tyr198 maintains its interaction with I:Tyr198, thus keeping the interface intact. An analysis of the distances between the aromatic rings of I:Trp175 and II:Tyr198 during the WT/WT and WT/W175A MD simulation supported our hypothesis. In the absence of II:Trp175, residue I:Trp175 moves closer to II:Tyr198, whereas the distance between I:Tyr198 II:Tyr198 does not change (Supplemental Fig. 4).

Discussion

It is now widely accepted that GPCRs can form oligomers, and a growing body of evidence points to the functional importance of oligomeric complexes for receptor trafficking, receptor activation, and G-protein coupling in native tissues (Rivero-Müller et al., 2010). The clinical significance of GPCR oligomerization has also become more evident during recent years, leading to identification of receptor oligomers as novel therapeutic targets (Waldhoer et al., 2005; González-Maeso et al., 2008). However, the lack of detailed structural information for GPCR dimers still raises an important challenge of understanding the functional role of oligomerization. Therefore, during the last decade, efforts were made to create models of GPCRs and their dimers by the use of computational simulations (Filizola and Weinstein, 2005; Casciari et al., 2008; Simpson et al., 2010; Johnston and Filizola, 2011) resulting in working models and testable hypotheses.

In the present work, we have combined computational and experimental procedures to investigate the 5-HT$_{1A}$ homodimerization. We have focused on the interaction interface within TM4 and TM5 and identified specific residues that are involved in the interaction between two monomeric units. It is noteworthy that the rationally designed mutations resulted in significantly decreased dimerization but did not completely prevent receptor-receptor interaction. This is in accord with the assumption that the 5-HT$_{1A}$ receptor can form higher-order oligomers (Ganguly et al., 2011). In this case, interface-disrupting mutations interfere with only one interface but allow interaction between two monomers on the other interface. Future investigation of additional interfaces will contribute to better understanding of the 5-HT$_{1A}$ oligomerization behavior.

Cellular Distribution of the Mutant 5-HT$_{1A}$ Receptors. It was important to identify mutated receptors that were localized at the plasma membrane to ensure that the receptors used in our study are mature, did not undergo structural deformation, and do not produce artifacts as a result of crowded environment. Indeed, some of the designed 5-HT$_{1A}$ receptor mutants did not reach the plasma membrane but instead remained in the intracellular compartments such as ER and/or Golgi (e.g., W136A/D140A; Table 2 and Fig. 2 and 3). Modified cellular distribution of GPCR mutants is important feature to receptor regulation and signaling (Jean-Alphonse and Hanyaloglu, 2011). It is noteworthy that several natural mutations of GPCRs that have pathophysiological implications also cause receptor retention within intracellular compartments (Bulenger et al., 2005). It has been shown that changing the hydrophobicity profile of residues, in particular Asp from the transmembrane region, can affect the transverse position of a corresponding TM helix and consequently affect the receptor distribution within the cell (Krishnakumar and London, 2007). Similar changes in the hydrophobicity profile may explain the disrupted membrane localization of the D140A mutant observed in the current work. We focused our studies on properly distributed mutants only.

Identified Interface Residues and Comparison to Other Family A GPCRs. We have identified residues involved in the interfaces between the 5-HT$_{1A}$ receptor monomers. It is noteworthy that some of these residues were previously mentioned to play a role in regulation of the 5-HT receptor functions. For example, the effect of Thr190$^{4.40}$ residue in 5-HT$_{2A}$ receptor on agonist induced receptor desensitization was described previously (Gray et al., 2003). In the case of the 5-HT$_{1A}$ receptor, Arg151$^{4.40}$ and Arg152$^{4.41}$ residues were suggested to be involved in the G-protein coupling (Kushwaha et al., 2006). Because these residues participate in receptor-receptor interaction interface, it will be interesting to study whether the decreased G-protein coupling obtained by Kushwaha et al. (2006) is due to impaired dimerization. To the best of our knowledge, residues Arg151$^{4.40}$, Arg152$^{4.41}$, Trp175$^{4.64}$, and Tyr198$^{5.41}$ were found for the first time to be involved in dimerization of 5-HT receptors and not to be involved in ligand binding. Residues flanking 5.41, such as Ser199$^{5.42}$ in the 5-HT$_{1A}$ receptor (Ho et al., 1992) and Ile199$^{5.40}$ in the 5-HT$_{1D}$ receptor (Wurch et al., 1998), were shown to be involved in ligand binding. This is in agreement with our structural model, in which both Trp175$^{4.64}$ and Tyr198$^{5.41}$ point to the dimerization interface and not into the binding pocket. Arg176$^{4.65}$ does point into the upper part of the TM core but it is not part of the binding site as defined either by (Yap et al., 2012) or by analogy to dopamine D$_3$ receptor binding site (Chien et al., 2010) (see Supplemental Fig. 1).

It is noteworthy that in δ-opioid receptor homodimeric complexes investigated by bioluminescence resonance energy transfer, cross-linking, and MD simulations, residue Ala163$^{4.40}$, which is equivalent to Arg151 in the 5-HT$_{1A}$ receptor, has been shown to take part in the proposed TM4 and TM4/TM5 interfaces, whereas Lys164$^{4.41}$, which is equivalent to Arg152 in the 5-HT$_{1A}$ receptor, participates in the proposed TM4/TM5 interface only. In contrast, residue Cys216$^{5.41}$, which is equivalent to Tyr198 in the 5-HT$_{1A}$ receptor, does not participate in the dimeric interfaces (Johnston et al., 2011).

After the completion of our current study, the structure of μ-opioid receptor (Manglik et al., 2012) joined the increasing numbers of structures of GPCRs in this exciting and ground breaking era of X-ray crystallography (Sprang, 2011; Steyaert and Kobilka, 2011; Katritch et al., 2012). The μ-opioid receptor molecules are associated into pairs along the crystallographic 2-fold axis through two different interfaces. One of the interfaces involves TM5 and TM6 and buried surface area of 1492 Å^2. This interface is suspected to be of biological relevance (Manglik et al., 2012). It is noteworthy that three monomers of serotonin have been found, in principle, to bind simultaneously, presenting both the μ-opioid receptor-like TM5/TM6 interface and the TM4/TM5 interface (analyzed in the current work), because there are no significant clashes in

such an arrangement (Supplemental Fig. 5). In high-order oligomers, both interfaces may take part.

Mutagenesis of Both Monomers. Our experimental results showed that in some cases, mutations of both monomers are needed to disrupt dimerization. We hypothesized that compensating interaction may occur between the mutant and the WT protomers but not in the mutant dimer. We used in silico mutagenesis and in vacuo 15-ns MD simulations to test this hypothesis. Indeed, the simulations provided possible explanations for the experimental results; i.e., in WT and W175A mutant dimerization, the distance between the remaining I:Trp175 residue and II:Tyr198 residue decreases after a few nanoseconds. This results in better positioning between the residues and allows stronger interactions. These suggestions will be tested in the future in experimental work and using additional simulation techniques, including explicit solvent, enhanced sampling and free energy simulations (Johnston and Filizola, 2011).

Relevance of Findings to Other Organisms and Other 5-HT$_1$ Subtypes. The amino acid sequence of the 5-HT$_{1A}$ receptor is highly conserved between species. In particular, Arg151$^{4.40}$, Arg152$^{4.41}$, Arg176$^{4.65}$, and Tyr198$^{5.41}$, which were found to be important for dimerization in the current work, are fully conserved in 18 representative species (including mammals, fish, and reptiles). It is noteworthy that Trp175$^{4.64}$ is conserved in 15 of the 18 species tested. Three fish sequences having a Met residue instead of Trp175$^{4.64}$ also have an insertion in EL2 (Supplemental Fig. 6). If 5-HT$_{1A}$ receptors in these species homodimerize, this might be achieved by a compensation for absence of Trp175$^{4.64}$ by interactions from the EL2 loop insertion. The residues we found to be pivotal for the 5-HT$_{1A}$ receptor dimerization, are conserved also in other 5-HT$_1$ receptor subtypes: Trp175$^{4.64}$, Arg176$^{4.65}$, and Tyr198$^{5.41}$. At position 4.40 (5-HT$_{1A}$ Arg151), there is a positively charged residue in four of the five 5-HT$_1$ sequences. At position 4.41 (5-HT$_{1A}$ Arg152), there is an Arg residue in 5-HT$_{1A}$, $_{1B}$, and $_{1E}$), whereas in 5-HT$_{1D}$ and 5-HT$_{1F}$, a His residue may also be positively charged (Supplemental Fig. 7). These results indicate a possibility for heterodimerization between different 5-HT$_1$ subtypes, which should be further investigated.

In summary, our work supports the transmembrane domains TM4/TM5 as the interface involved in dimerization of the 5-HT$_{1A}$ receptor. Residues Trp175$^{4.64}$, Tyr198$^{5.41}$, Arg151$^{4.40}$, and Arg152$^{4.41}$ were computationally predicted and experimentally confirmed to be important for the interaction interface. Because the 5-HT$_{1A}$ mutants designed and characterized in this work show significantly reduced dimerization, they can be used to investigate the functional importance of the 5-HT$_{1A}$ receptor dimerization. This will aid in studying the role of dimerization in 5-HT$_{1A}$ receptor mediated signal transduction and facilitate further studies of 5-HT$_{1A}$ receptor oligomerization and heterodimerization of 5-HT$_{1A}$ with other receptors.

Acknowledgments

We thank Dr. Talia Yarnitzky for helpful discussions.

Authorship Contributions

Participated in research design: Kowalsman, Seifert, Ponimaskin, and Niv.

Conducted experiments: Gorinski, Kowalsman, Renner, Wirth, Reinartz, Zeug, and Niv.

Contributed new reagents or analytic tools: Zeug.

Performed data analysis: Kowalsman, Gorinski, Reinartz, Zeug, Ponimaskin, and Niv.

Wrote or contributed to the writing of the manuscript: Kowalsman, Ponimaskin, and Niv.

References

Albizu L, Cottet M, Kralikova M, Stoev S, Seyer R, Brabet I, Roux T, Bazin H, Bourrier E, Lamarque L, et al. (2010) Time-resolved FRET between GPCR ligands reveals oligomers in native tissues. *Nat Chem Biol* **6:**587–594.
Alva V, Syamala Devi DP, and Sowdhamini R (2008) COILCHECK: an interactive server for the analysis of interface regions in coiled coils. *Protein Pept Lett* **15:**33–38.
Bahadur RP, Chakrabarti P, Rodier F, and Janin J (2003) Dissecting subunit interfaces in homodimeric proteins. *Proteins* **53:**708–719.
Ballesteros J and Weinstein H (1995) Integrated methods for the construction of three-dimensional models and computational probing of structure-function relations in G protein-coupled receptors. *Methods Neurosci* **25:**366–428.
Brooks BR, Brooks CL 3rd, Mackerell AD Jr, Nilsson L, Petrella RJ, Roux B, Won Y, Archontis G, Bartels C, Boresch S, et al. (2009) CHARMM: the biomolecular simulation program. *J Comput Chem* **30:**1545–1614.
Bulenger S, Marullo S, and Bouvier M (2005) Emerging role of homo- and heterodimerization in G-protein-coupled receptor biosynthesis and maturation. *Trends Pharmacol Sci* **26:**131–137.
Camacho CJ and Zhang C (2005) FastContact: rapid estimate of contact and binding free energies. *Bioinformatics* **21:**2534–2536.
Casciari D, Dell'Orco D, and Fanelli F (2008) Homodimerization of neurotensin 1 receptor involves helices 1, 2, and 4: insights from quaternary structure predictions and dimerization free energy estimations. *J Chem Inf Model* **48:**1669–1678.
Chien EY, Liu W, Zhao Q, Katritch V, Han GW, Hanson MA, Shi L, Newman AH, Javitch JA, Cherezov V, et al. (2010) Structure of the human dopamine D3 receptor in complex with a D2/D3 selective antagonist. *Science* **330:**1091–1095.
de Vries SJ, van Dijk M, and Bonvin AM (2010) The HADDOCK web server for data-driven biomolecular docking. *Nat Protoc* **5:**883–897.
Fernandez-Fuentes N, Rai BK, Madrid-Aliste CJ, Fajardo JE, and Fiser A (2007) Comparative protein structure modeling by combining multiple templates and optimizing sequence-to-structure alignments. *Bioinformatics* **23:**2558–2565.
Filizola M and Weinstein H (2005) The study of G-protein coupled receptor oligomerization with computational modeling and bioinformatics. *FEBS J* **272:**2926–2938.
Fotiadis D, Liang Y, Filipek S, Saperstein DA, Engel A, and Palczewski K (2003) Atomic-force microscopy: Rhodopsin dimers in native disc membranes. *Nature* **421:**127–128.
Ganguly S, Clayton AH, and Chattopadhyay A (2011) Organization of higher-order oligomers of the serotonin$_{1A}$ receptor explored utilizing homo-FRET in live cells. *Biophys J* **100:**361–368.
González-Maeso J, Ang RL, Yuen T, Chan P, Weisstaub NV, López-Giménez JF, Zhou M, Okawa Y, Callado LF, Milligan G, et al. (2008) Identification of a serotonin/glutamate receptor complex implicated in psychosis. *Nature* **452:**93–97.
Gray JA, Compton-Toth BA, and Roth BL (2003) Identification of two serine residues essential for agonist-induced 5-HT2A receptor desensitization. *Biochemistry* **42:**10853–10862.
Guo W, Shi L, Filizola M, Weinstein H, and Javitch JA (2005) Crosstalk in G protein-coupled receptors: changes at the transmembrane homodimer interface determine activation. *Proc Natl Acad Sci USA* **102:**17495–17500.
Guo W, Shi L, and Javitch JA (2003) The fourth transmembrane segment forms the interface of the dopamine D2 receptor homodimer. *J Biol Chem* **278:**4385–4388.
Ho BY, Karschin A, Branchek T, Davidson N, and Lester HA (1992) The role of conserved aspartate and serine residues in ligand binding and in function of the 5-HT1A receptor: a site-directed mutation study. *FEBS Lett* **312:**259–262.
Hoyer D, Pazos A, Probst A, and Palacios JM (1986) Serotonin receptors in the human brain. I. Characterization and autoradiographic localization of 5-HT1A recognition sites. Apparent absence of 5-HT1B recognition sites. *Brain Res* **376:**85–96.
Hu J, Thor D, Zhou Y, Liu T, Wang Y, McMillin SM, Mistry R, Challiss RA, Costanzi S, and Wess J (2012) Structural aspects of M3 muscarinic acetylcholine receptor dimer formation and activation. *FASEB J* **26:**604–616.
Humphrey W, Dalke A, and Schulten K (1996) VMD: visual molecular dynamics. *J Mol Graph* **14:**33–38.
Ishida T and Kinoshita K (2007) PrDOS: prediction of disordered protein regions from amino acid sequence. *Nucleic Acids Res* **35:**W460–W464.
James JR, Oliveira MI, Carmo AM, Iaboni A, and Davis SJ (2006) A rigorous experimental framework for detecting protein oligomerization using bioluminescence resonance energy transfer. *Nat Methods* **3:**1001–1006.
Jean-Alphonse F and Hanyaloglu AC (2011) Regulation of GPCR signal networks via membrane trafficking. *Mol Cell Endocrinol* **331:**205–214.
Johnston JM, Aburi M, Provasi D, Bortolato A, Urizar E, Lambert NA, Javitch JA, and Filizola M (2011) Making structural sense of dimerization interfaces of delta opioid receptor homodimers. *Biochemistry* **50:**1682–1690.
Johnston JM and Filizola M (2011) Showcasing modern molecular dynamics simulations of membrane proteins through G protein-coupled receptors. *Curr Opin Struct Biol* **21:**552–558.
Jones S and Thornton JM (1996) Principles of protein-protein interactions. *Proc Natl Acad Sci USA* **93:**13–20.
Katritch V, Cherezov V, and Stevens RC (2012) Diversity and modularity of G protein-coupled receptor structures. *Trends Pharmacol Sci* **33:**17–27.
Khawaja X, Ennis C, and Minchin MC (1997) Pharmacological characterization of

recombinant human 5-hydroxytryptamine1A receptors using a novel antagonist radioligand, [3H]WAY-100635. *Life Sci* **60:**653–665.
Kobe F, Renner U, Woehler A, Wlodarczyk J, Papusheva E, Bao G, Zeug A, Richter DW, Neher E, and Ponimaskin E (2008) Stimulation- and palmitoylation-dependent changes in oligomeric conformation of serotonin 5-HT1A receptors. *Biochim Biophys Acta* **1783:**1503–1516.
Kortemme T, Kim DE, and Baker D (2004) Computational alanine scanning of protein-protein interfaces. *Sci STKE* **2004:**pl2.
Krishnakumar SS and London E (2007) The control of transmembrane helix transverse position in membranes by hydrophilic residues. *J Mol Biol* **374:**1251–1269.
Krissinel E and Henrick K (2007) Inference of macromolecular assemblies from crystalline state. *J Mol Biol* **372:**774–797.
Kushwaha N, Harwood SC, Wilson AM, Berger M, Tecott LH, Roth BL, and Albert PR (2006) Molecular determinants in the second intracellular loop of the 5-hydroxytryptamine-1A receptor for G-protein coupling. *Mol Pharmacol* **69:**1518–1526.
Lam DD and Heisler LK (2007) Serotonin and energy balance: molecular mechanisms and implications for type 2 diabetes. *Expert Rev Mol Med* **9:**1–24.
Lerch-Bader M, Lundin C, Kim H, Nilsson I, and von Heijne G (2008) Contribution of positively charged flanking residues to the insertion of transmembrane helices into the endoplasmic reticulum. *Proc Natl Acad Sci USA* **105:**4127–4132.
Lesch KP and Gutknecht L (2004) Focus on The 5-HT1A receptor: emerging role of a gene regulatory variant in psychopathology and pharmacogenetics. *Int J Neuropsychopharmacol* **7:**381–385.
Levit A, Barak D, Behrens M, Meyerhof W, and Niv MY (2012) Homology model-assisted elucidation of binding sites in GPCRs. *Methods Mol Biol*, in press.
Liang Y, Fotiadis D, Filipek S, Saperstein DA, Palczewski K, and Engel A (2003) Organization of the G protein-coupled receptors rhodopsin and opsin in native membranes. *J Biol Chem* **278:**21655–21662.
Lohse MJ (2010) Dimerization in GPCR mobility and signaling. *Curr Opin Pharmacol* **10:**53–58.
Mancia F, Assur Z, Herman AG, Siegel R, and Hendrickson WA (2008) Ligand sensitivity in dimeric associations of the serotonin 5HT2c receptor. *EMBO Rep* **9:**363–369.
Manglik A, Kruse AC, Kobilka TS, Thian FS, Mathiesen JM, Sunahara RK, Pardo L, Weis WI, Kobilka BK, and Granier S (2012) Crystal structure of the μ-opioid receptor bound to a morphinan antagonist. *Nature* **485:**321–326.
Meyer BH, Segura JM, Martinez KL, Hovius R, George N, Johnsson K, and Vogel H (2006) FRET imaging reveals that functional neurokinin-1 receptors are monomeric and reside in membrane microdomains of live cells. *Proc Natl Acad Sci USA* **103:**2138–2143.
Milligan G (2009) G protein-coupled receptor hetero-dimerization: contribution to pharmacology and function. *Br J Pharmacol* **158:**5–14.
Niv MY and Filizola M (2008) Influence of oligomerization on the dynamics of G-protein coupled receptors as assessed by normal mode analysis. *Proteins* **71:**575–586.
Niv MY, Skrabanek L, Filizola M, and Weinstein H (2006) Modeling activated states of GPCRs: the rhodopsin template. *J Comput Aided Mol Des* **20:**437–448.
Niv MY and Weinstein H (2005) A flexible docking procedure for the exploration of peptide binding selectivity to known structures and homology models of PDZ domains. *J Am Chem Soc* **127:**14072–14079.
Paila YD, Kombrabail M, Krishnamoorthy G, and Chattopadhyay A (2011a) Oligomerization of the serotonin(1A) receptor in live cells: a time-resolved fluorescence anisotropy approach. *J Phys Chem B* **115:**11439–11447.
Paila YD, Tiwari S, Sengupta D, and Chattopadhyay A (2011b) Molecular modeling of the human serotonin(1A) receptor: role of membrane cholesterol in ligand binding of the receptor. *Mol Biosyst* **7:**224–234.
Pulagam LP and Palczewski K (2010) Electrostatic compensation restores trafficking of the autosomal recessive retinitis pigmentosa E150K opsin mutant to the plasma membrane. *J Biol Chem* **285:**29446–29456.
Renner U, Glebov K, Lang T, Papusheva E, Balakrishnan S, Keller B, Richter DW, Jahn R, and Ponimaskin E (2007) Localization of the mouse 5-hydroxytryptamine(1A) receptor in lipid microdomains depends on its palmitoylation and is involved in receptor-mediated signaling. *Mol Pharmacol* **72:**502–513.
Renner U, Zeug A, Woehler A, Niebert M, Dityatev A, Dityateva G, Gorinski N, Guseva D, Abdel-Galil D, Fröhlich M, et al. (2012) Heterodimerization of serotonin receptors 5-HT1A and 5-HT7 differentially regulates receptor signalling and trafficking. *J Cell Sci* http://dx.doi.org/10.1242/jcs.101337.
Reynolds C, Damerell D, and Jones S (2009) ProtorP: a protein-protein interaction analysis server. *Bioinformatics* **25:**413–414.
Richter DW, Manzke T, Wilken B, and Ponimaskin E (2003) Serotonin receptors: guardians of stable breathing. *Trends Mol Med* **9:**542–548.
Rivero-Müller A, Chou YY, Ji I, Lajic S, Hanyaloglu AC, Jonas K, Rahman N, Ji TH, and Huhtaniemi I (2010) Rescue of defective G protein-coupled receptor function in vivo by intermolecular cooperation. *Proc Natl Acad Sci USA* **107:**2319–2324.
Roy A, Kucukural A, and Zhang Y (2010) I-TASSER: a unified platform for automated protein structure and function prediction. *Nat Protoc* **5:**725–738.
Rozenfeld R and Devi LA (2011) Exploring a role for heteromerization in GPCR signalling specificity. *Biochem J* **433:**11–18.
Simpson LM, Taddese B, Wall ID, and Reynolds CA (2010) Bioinformatics and molecular modelling approaches to GPCR oligomerization. *Curr Opin Pharmacol* **10:**30–37.
Sprang SR (2011) Cell signalling: binding the receptor at both ends. *Nature* **469:**172–173.
Steyaert J and Kobilka BK (2011) Nanobody stabilization of G protein-coupled receptor conformational states. *Curr Opin Struct Biol* **21:**567–572.
Veatch W and Stryer L (1977) The dimeric nature of the gramicidin A transmembrane channel: conductance and fluorescence energy transfer studies of hybrid channels. *J Mol Biol* **113:**89–102.
Vroling B, Sanders M, Baakman C, Borrmann A, Verhoeven S, Klomp J, Oliveira L, de Vlieg J, and Vriend G (2011) GPCRDB: information system for G protein-coupled receptors. *Nucleic Acids Res* **39:**D309–D319.
Waldhoer M, Fong J, Jones RM, Lunzer MM, Sharma SK, Kostenis E, Portoghese PS, and Whistler JL (2005) A heterodimer-selective agonist shows in vivo relevance of G protein-coupled receptor dimers. *Proc Natl Acad Sci USA* **102:**9050–9055.
Wang HX and Konopka JB (2009) Identification of amino acids at two dimer interface regions of the alpha-factor receptor (Ste2). *Biochemistry* **48:**7132–7139.
Wlodarczyk J, Woehler A, Kobe F, Ponimaskin E, Zeug A, and Neher E (2008) Analysis of FRET signals in the presence of free donors and acceptors. *Biophys J* **94:**986–1000.
Woehler A, Wlodarczyk J, and Ponimaskin EG (2009) Specific oligomerization of the 5-HT1A receptor in the plasma membrane. *Glycoconj J* **26:**749–756.
Wurch T, Colpaert FC, and Pauwels PJ (1998) Chimeric receptor analysis of the ketanserin binding site in the human 5-hydroxytryptamine(1D) receptor: importance of the second extracellular loop and fifth transmembrane domain in antagonist binding. *Mol Pharmacol* **54:**1088–1096.
Yap BK, Buckle MJ, and Doughty SW (2012) Homology modeling of the human 5-HT(1A), 5-HT (2A), D1, and D2 receptors: model refinement with molecular dynamics simulations and docking evaluation. *J Mol Model* http://dx.doi.org/10.1007/s00894-012-1368-5.
Yarnitzky T, Levit A, and Niv MY (2010) Homology modeling of G-protein-coupled receptors with X-ray structures on the rise. *Curr Opin Drug Discov Devel* **13:**317–325.

Address correspondence to: Dr. Masha Niv, Institute of Biochemistry, Food Science and Nutrition and the Fritz Haber Center for Molecular Dynamics, the Hebrew University of Jerusalem, Israel. E-mail: niv@agri.huji.ac.il